Förderschwerpunkt Photonik

**Teilvorhaben:** Leucht- und Laserdioden für die optische Kommunikationstechnik bei Wellenlängen oberhalb 2 µm

**Zuwendungsempfänger:** Fraunhofer-Gesellschaft
Institut für Angewandte Festkörperphysik

**Förderkennzeichen:** 01 BP 704A

**Laufzeit:** 01.09.2000 - 31.08.2003

**Projektleiter:** Prof. J. Wagner

**Bearbeiter:**
Dr. F. Fuchs
Dr. N. Herres (bis 05.2001)
Dr. L. Kirste (seit 04.2001)
Dr. R. Kiefer
Dr. C. Mermelstein
Dr. W. Pletschen
Dr. M. Rattunde
Dr. J. Schmitz
Dr. M. Walther

December 2003

# Contents

Wissenschaftlich-technische Ergebnisse

# I. GaInAsSb/AlGaAsSb-based type-I diode lasers

## 1. Introduction

Due to the worldwide interest in infrared LEDs and diode lasers with emission wavelength above 2 µm for the optical free space communication, significant efforts are devoted to investigate new materials as well as new laser structure concepts. Moreover, this application requires robust, compact and reliable infrared laser light sources. On the basis of III-V compound semiconductor quantum structures, such lasers have been realized employing different device concepts. Within the current project antimonide-based III-V semiconductor diode lasers have been developed, with targeted purpose as direct implementation in the free space communication applications for the mid-infrared spectral interval above 2 µm. The III-V (AlGaIn)(AsSb) semiconductor materials system is favorably suitable for the fabrication of this sort of LEDs and diode lasers. Employing quaternary alloys the GaInAsSb semiconductor band gap can be tuned between 0.3 and 0.7 eV, which corresponds to a wavelength range between 1.7 and 4.2 µm. This can be realized simply by varying the alloy composition. Besides, using quaternary compounds the lattice constant can be adjusted as well, so that lattice matched as well as strained layers can be grown on the GaSb substrate.

For the wavelength range spanning from 2 to 3 µm the type-I diode laser concept with GaInAsSb/AlGaAsSb quantum wells (QWs) as active region is employed. In the type-I laser structures the electrical carriers, namely the electrons and holes, are localized in the same epitaxial layer, in this case in the GaInAsSb QW layer, and a spatially direct recombination process takes place generating the desired light emission. For the next longer wavelength interval, 3 to 5 µm, the InAs/GaInSb/AlGaAsSb type-II W-laser concept has been employed. In this configuration the electrons and holes are located in adjacent epitaxial layers, i.e. in the InAs and GaInSb, respectively, resulting in a spatially indirect recombination process for the infrared light emission. The type-II laser is described in details in the second part of the present report.

The growth of the epitaxial layer sequence for both diode laser concepts was realized using two growth techniques, the Molecular Beam Epitaxy (MBE) and the Metal Organic Vapor Deposition (MOCVD), in both cases on GaSb substrates. The research at IAF was accompanied by a study regarding MOCVD growth of group III-(AsNSb) structures, conducted by Prof. Dan Fekete at the Technion-Haifa (Israel) carried out as a subcontract of the current project. In terms of material quality, straight away after growth the epitaxial layers were on wafer-level characterized using ex-situ high resolution X-ray diffraction (HRXRD), secondary ion mass spectroscopy (SIMS) as well as photoluminescence spectroscopy (PL). For the fabrication of the optical active region of the laser structures, GaInAsSb/AlGaAsSb quantum layers and InAs/GaInSb/AlGaAsSb

layer sequences have been used for the type-I and type-II lasers respectively. In the type-I layer structures the GaInAsSb QW-layers are separated by lattice matched AlGaAsSb barrier layers with Al-content varying between 20-40%. For the type-II laser structures the InAs/GaInSb/InAs QW triple-layers are separated by low Al-content AlGaAsSb interperiod barriers. For both laser types the active region is embedded between low Al-content AlGaAsSb separate confinement layers resulting in a broadened waveguide design. The waveguide core in turn is sandwiched between high Al-content AlGaAsSb optical cladding layers with Al-content about 85%, again lattice matched to the GaSb substrate. The cladding material alloy has a high energy gap and therefore a low refractive index, condition requested for a good wave guiding.

## 2. Diode lasers emitting between 1.7 – 2.34 µm

With a first series of samples, GaInAsSb/AlGaAsSb diode lasers with emission wavelengths between 1.7 and 2.34 µm have been investigated. A detailed study related to the temperature dependence of the threshold current as a function of the wavelength has been conducted, by comparing a set of ten different laser structures. Additionally, the laser characteristic parameters, including the characteristic temperature $T_0$, the internal quantum efficiency $\eta_i$, and the internal loss coefficient $\alpha_i$ have been deduced. Electro-optical characterization in cw mode has been performed for the whole set of diode lasers. In addition, pulsed measurements have been carried out to determine the pulsed threshold current, using 5 µs short pulses at 10 kHz repetition rate, in order to avoid self-heating of the devices. The light output power as a function of the drive current was measured at heat sink temperatures between 250 and 360 K for several ridge widths and cavity lengths.

The laser structures under investigation were grown by solid-source MBE on (100) oriented n-type GaSb:Te substrates. The active region of this set of ten lasers consists of three compressively strained 10 nm thick $Ga_{1-x}In_xAs_ySb_{1-y}$ QWs, with $0.16 \leq x \leq 0.30$ and $0 \leq y \leq 0.15$, separated by 20 nm thick $Al_{0.29}Ga_{0.71}As_{0.02}Sb_{0.98}$ barriers lattice matched to the GaSb substrate. The QW region is embedded between 400 nm thick $Al_{0.29}Ga_{0.71}As_{0.02}Sb_{0.98}$ separate confinement layers (SCLs) and sandwiched between n- and p-doped 2 µm wide $Al_{0.84}Ga_{0.16}As_{0.06}Sb_{0.94}$ optical cladding layers. The growth is completed by a $p^+$- GaSb contact layer. All epitaxial layers except the QWs were grown nominally lattice matched to the GaSb buffer layer. Following epitaxial growth the wafers were analyzed by high-resolution X-ray diffraction (HRXRD), photoluminescence (PL) spectroscopy and secondary ion mass spectrometry (SIMS) in order to determine the strains and compositions of the individual layers, the PL emission profile and peak wavelength, as well as the doping concentrations, respectively. Edge-emitting index-guided Fabry-Perot diode lasers with ridge widths varying from 6 to 64 µm have been prepared using standard optical lithography and chemically assisted ion beam etching (CAIBE). Ti/Pt/Au and (AuSn)Au have been deposited for the top p-contact and backside n-contact metallization, respectively. Laser bars with cavity lengths varying between 0.5 and 2 mm were cleaved and soldered either substrate-side down or, for higher output powers, epi-side down onto copper heat sinks. For several laser bars, to maximize single

ended output, low-reflectivity, AR (5%), and high-reflectivity, HR (95%), coatings were applied to the cleaved mirror facets.

The 280 K cw lasing spectra corresponding to the ten different diode lasers spanning the 1.7 - 2.34 µm spectral range are shown in Figure 1. These spectra were obtained for 64 µm x 600 µm ridge geometry and cw drive currents slightly above threshold. Several devices exhibited single mode lasing emission, while multi-mode behavior emerged at higher currents. The inset displays the spectrum of the 2.13 µm laser on an expanded wavelength scale, showing well resolved multiple longitudinal modes with ~1 nm mode spacing. The thermal red shift of the emission wavelength amounted to ~1.3 nm/°C due to the shift of the gain peak.

Figure 2 illustrates representative cw power output and total power efficiency plotted versus injection current, recorded at 280 K heat sink temperature for three different diode lasers emitting at 1.94, 2.21 and 2.34 µm, all having a 64 µm x 1000 µm size. As clearly seen in the plot, the light output power drops substantially upon increasing the wavelength, so does the power efficiency, due to the increase of Auger losses and QW heterobarrier carrier leakage with increasing wavelength. The maximum output powers are limited by the onset of thermal rollover due to the substrate-side down mounting of the devices. The maximum output power decreases approximately by a factor of three when proceeding from the shortest to the longest wavelength device, accompanied by a decrease in maximum power efficiency from 29% to 10%.

Higher light output powers have been obtained by applying HR/AR coating with reflectivities of 97% and 6%, respectively, to the mirror facets of the lasers. Figure 3 depicts the cw power output and total power efficiency versus injection current at 280 K of two 64 µm x 1000 µm ridge waveguide lasers with uncoated and HR/AR coated mirror facets, both emitting at 1.94 µm. A cw output power of 388 mW was achieved for the coated laser in comparison with just 173 mW/facet for the laser without coating, at the same drive current of 1.54 A. The maximum total power efficiency (power emitted by both facets of the uncoated device) amounted to 29% for the uncoated laser and a comparable value of 27% for the coated one. The slight difference between these two values is due to the scatter between different devices.

## 3. Wavelength dependence of the characteristic temperature $T_o$

A detailed study was carried out regarding the characteristic temperature $T_O$ of the threshold current by characterizing the devices in cw as well as in pulsed operation. Representative results for the temperature dependence of the threshold current $I_{th}$ measured in pulsed mode are depicted in Figure 4, for four different lasers with emission wavelength of 2.34, 2.30, 2.13 and 1.94 µm. For the three diode lasers emitting on the short-wavelength side two distinct temperature intervals are visible showing different $T_O$ values. We found that in the low temperature regime $T_O$ decreases from 179 K to 54 K when proceeding from the 1.94 µm to the 2.34 µm device.

In order to understand this decrease of $T_O$ with increasing wavelength, it is necessary to analyze the two main contributions responsible for the temperature sensitivity of $I_{th}$, i.e. the Auger recombination and the heterobarrier carrier leakage. The Auger recombination rate is proportional to $\exp(-\mu \cdot E_g / k \cdot T)$, where $E_g$ is the effective band gap energy and μ designates the reduced electron-hole mass. Therefore, if Auger is the dominant loss mechanism, $T_O$ is expected to increase with the band gap. To test the validity of this assumption for the present set of lasers, $T_O$ (for the low-temperature range) is plotted in Figure 5 against the emitted photon energy. In order to provide a higher accuracy of the experimental data, $T_O$ values obtained from pulsed measurements have been used since they are more precise than cw measurements, as the former measurement mode prevents self-heating of the devices. Indeed, as shown in Figure 5 for samples A to G, an increase in $T_O$ with photon energy is observed as expected from the above discussion, but all at once a drop for lasers H, I and J, emitting on the short-wavelength side, appears which is not consistent with the view of Auger recombination limited threshold current. On the other hand, the heterobarrier leakage is proportional to $m^{-1/2} \cdot \exp(-E_B/kT)$, where $E_B$ is the conduction ($\Delta E_C$) or valence band offset ($\Delta E_V$), whatever is smaller, and m is the effective electron or hole mass, whatever concerns. Therefore, if the heterobarrier leakage is the dominant mechanism, $T_O$ should increase with $E_B$. Figure 6 displays the $T_O$ values as a function of the conduction or valence band offset, whichever is smaller. Within the scatter of the experimental data a monotonic increase of $T_O$ with increasing band offset is observed, favoring the assumption that heterobarrier leakage is indeed dominant. Detailed studies of GaInAsSb/AlGaAsSb type-I QW diode lasers emitting in the 2.3 to 2.6 μm wavelength range have shown that for 2.3 μm lasers with $\Delta E_C \approx \Delta E_V$, the temperature dependence of $I_{th}$ is governed by monomolecular nonradiative recombination [D. Garbuzov et al., Appl. Phys. Lett. 74, 2990 (1999)]. Therefore, the current experimental results lead us to conclude that of the two mechanisms discussed above, the temperature dependence of $I_{th}$ is governed by heterobarrier carrier leakage, limiting the high-temperature performance of the present diode lasers.

To deduce the standard laser parameters, i.e. the internal quantum efficiency ($\eta_i$) and internal loss coefficient ($\alpha_i$), experiments including different cavity lengths were performed. The external quantum efficiency ($\eta_d$) was measured for a series of seven cavity lengths varying between 0.5 - 2 mm. The $\eta_i$ and $\alpha_i$ values were derived using the relation $\eta_d = \eta_i / [1+\alpha_i L/\ln(1/R)]$. Table I summarizes the laser parameters, $\alpha_i$, $\eta_i$ and $J_{th}$ for infinite cavity length ($J_{th,\infty}$), derived for the present series of diode lasers emitting between 1.7 and 2.34 μm. For sample I, however, the cavity length dependence of $\eta_d$ was not fully consistent and did not permit extraction of the internal loss and internal efficiency. However, $J_{th}$ for infinite cavity length could be determined reliably and amounted to 155 A/cm$^2$. All the results were obtained for a 64 μm aperture, measured at 280 K heat sink temperature.

## 4. Beam quality as measured by far field beam profile

The transversal optical field has been calculated taking into account the various refractive indexes of the different epitaxial layers forming the optical waveguide. Figure 7 shows the refractive index profile and the resulting transversal optical mode intensity distribution as a function of the transversal position, corresponding to the growth direction, for two different diode lasers emitting at 1.84 and 2.34 µm. The inset displays the same data on an expanded length scale for the active region. The calculated confinement factor of the QWs (defined by the overlap between the optical mode and the QWs) amounts to 4.7% for the 1.84 µm laser and 4% for the 2.34 µm device. The overlap with the cladding layers was calculated as well, yielding values of 8.7% and 15.5% for the short and long wavelength emitting devices, respectively.

An additional important issue for free space optical communication is the beam quality. To that purpose the far field (FF) distribution both along the slow and fast axis have been measured. FF scans in the transversal (fast axis) and lateral direction (slow axis) of the laser emission have been performed by rotating the diode laser placed at a distance of 20 cm in front of an extended wavelength InGaAs detector with 1 mm aperture. The diode laser has been operated at two different drive currents, 2 and 4 times the threshold. The device under investigation had a 16 µm x 1000 µm geometry and the mirror facets were HR/AR coated. All the measurements were performed at room temperature. The measured fast axis profiles for the two different injection currents, $2I_{th}$ and $4I_{th}$, were almost identical, exhibiting a Gaussian shape with full-width at half-maximum (FWHM) divergence angle of ~ 67°, which compares well with the calculated value of 60°. Figure 8 displays the calculated and measured transversal FF angular distribution for the above-mentioned diode lasers, emitting at 1.84 and 2.34 µm. The graph reveals a very good agreement between the calculated and experimental data. In addition, both the calculated and simulated curves show no significant dependence on the wavelength.

The lateral optical field was calculated for a diode laser emitting at 1.94 µm with 16 µm wide ridge geometry. Figure 9 presents the calculated lateral optical mode profile (right axis) up to the $2^{nd}$ order, together with the effective refractive index (left axis) reflecting the rectangular shape of the 16 µm ridge aperture. In contrast to the transversal pattern, however, the lateral optical distribution shows a multi-mode behavior.

Figure 10 illustrates the angular dependence of the measured (upper) and simulated (lower) lateral FF intensities of the 1.94 µm diode laser with 16 µm ridge width and 1000 µm cavity length. The measurements have been performed again at $2I_{th}$ and $4I_{th}$. Upon increasing the injection current, the profile shape changes, showing higher order side peaks, and the FWHM of the divergence angle increases somewhat from 4.8° ($2I_{th}$) to 5.6° ($4I_{th}$). Regarding the measured profiles, at $2I_{th}$ only the zero order mode is visible in the experimental FF profile, whereas at $4I_{th}$ the first and second order modes are clearly resolved. The angular dependence of the lateral FF was calculated up to the 3rd order mode. The angular position of the measured side peaks originating from higher order modes is in excellent agreement with the calculations.

## 5. Thermally activated heterobarrier carrier leakage

In the following, the heterobarrier leakage due to thermally activated carriers has been investigated in more detail. By increasing the Al concentration in the barriers and SCLs, a higher band offset in both the conduction and valence band is formed leading to an improved carrier confinement and to a suppressed heterobarrier leakage. Figure 11 shows the energy band-edge profile of three different laser structures calculated using the Model Solid Theory [M. P. C. M. Krijn, Semicond. Sci. Technol. 6, 27 (1991)]. For the purpose of this study, diode lasers with same emission wavelength but different band offsets, realized by varying the Al-content in the barriers and SCLs, were grown and characterized. A series of three diode lasers designed for 2.23 µm emission wavelength with three $Ga_{0.70}In_{0.30}As_{0.08}Sb_{0.92}$ QWs were grown, varying the Al-composition (20%, 30% and 40%) in the barriers and SCLs while keeping both lattice matched to the GaSb buffer layer. The other parts of the structure remained identical to the set of diode lasers described in part 2 of this section.

The transversal optical field distribution was calculated taking into account the various refractive indexes of the different epitaxial layers forming the optical waveguide. Figure 12 (a) shows the refractive index and the resulting transversal optical mode intensity with respect to the transversal position, corresponding to the growth direction, for three diode lasers with different Al-concentrations in barriers and SCLs of 20%, 30%, and 40%, respectively. All three devices had an emission wavelength of 2.23 µm. Figure 12 (b) represents a zoomed graph of the active region. The calculated confinement factor of the QWs (defined as the overlap of the optical mode with the QWs) amounts to 4.3% for the 20% Al device and decreases gradually to 4.1% and 3.9% for the respective higher Al concentration devices. However, the confinement factor of the cladding layers reveals an opposite behavior, increasing from 11.6% to 17% with increasing Al concentration.

Figure 13 illustrates the cw output power vs current characteristics for three 64 µm x 1000 µm lasers, each with different Al-composition. These results were obtained for 280 K heat sink temperature. We find that the threshold current of the 20% and 30% Al-content lasers are comparable, however a substantial increase by about a factor of two is obtained for the 40% Al laser. This significant increase of $I_{th}$ may be attributed to the crossover of the $\Gamma$ and L conduction bands minima with the X minima, which occurs at Al compositions of around 40% in ternary AlGaSb alloys. This crossover is expected to have an effect because inter-valley scattering is required for electron capture into the QW.

As shown in Figure 14 (a), a maximum total power efficiency of 30% is achieved for the 20% Al-content laser, representing a record high value for 2.23 µm emission wavelength. The power efficiency degrades with increasing Al-content, as a result of increased operating voltages. The corresponding voltage-current characteristics for the three different diode lasers are illustrated in Figure 14 (b), revealing an increase in the turn-on voltage when proceeding from the low to high Al-concentration in the devices, as expected due to higher band offsets, and thus larger band gap energies in the barriers and SCLs.

The temperature dependence of the threshold current for the three different Al-content diode lasers measured in pulsed operation is shown in Figure 15. A high characteristic temperature $T_O = 93$ K is achieved for the 40% Al-content device in the complete temperature range, while for the lower Al-content devices two distinctive regimes are observable, yielding lower $T_O$ values above 310 K, as indicated in the graph. We find that for the high temperature range from 250 to 360 K, the device with 40% Al has a major advantage regarding $T_O$ as compared to those with 20% and 30% Al with $T_O$ values of 63 and 66 K, respectively. The high $T_O$ is associated with a better carrier confinement, leading to reduced heterobarrier leakage losses in the laser structure. In conclusion, the high $T_O$ value correlates with the increased band offsets in both the conduction ($\Delta E_C$) and valence bands ($\Delta E_V$).

Furthermore, all three devices exhibited low internal loss coefficients of 6.3 $cm^{-1}$ (20% Al), 6.8 $cm^{-1}$ (30% Al) and 6.2 $cm^{-1}$ (40% Al) and high internal efficiencies of 83% (20%, 40% Al) and 89% (30% Al), reflecting the superior material quality of these diode lasers.

## 6. Development of GaInAsSb/AlGaAsSb laser core structures for emission towards 2.7 µm

Longer emission wavelength diode lasers towards 2.7 µm with GaInAsSb QWs can in principal be realized by increasing the As-content in the QWs, but this reduces the valence band offset significantly. As shown above in sections 3 and 5, both the conduction band offset as well as the valence band offset have to be as large as possible, i.e. $\Delta E_C \approx \Delta E_V = E_g/2$ for good device performances. Therefore, the following development strategy has been pursued for the realization of GaInAsSb type-I QW diode lasers with emission wavelength > 2.3 µm.

The concept we adopted to achieve longer lasing wavelength was the following: increase the In-content in the QWs while keeping the As-concentration at a fix value until the structure exhibits strain relaxation. After then, as next step the As-content was set to a higher value and over again, i.e. to grow several core test structures by successively increasing the In-content in the QWs till strain relaxation begins. Following this iteration several times laser core test structure with emission at 2.7 µm should be realized. Figure 16 shows the calculated conduction and valence band potentials for three different QWs. Using different In and As compositions in the QWs the transition energy varies from 2 µm (a) to 2.4 µm ((b) and (c)). Basically, the emission wavelength is determined by the In- and As-concentration in the QWs, however, there is a trade-off between longer wavelength and week carrier confinement due to small band offsets in particular in the valence band. Thus, the approach is as mentioned already above to increase the In-content and keep the As concentration as low as possible to prevent strain relaxation.

For the development of type-I diode lasers with emission wavelength towards 2.7 µm, laser core test structures comprising five QWs have been grown and the epitaxial material was characterized. The test structures grown by MBE consist of five 10 nm

thick GaInAsSb compressively strained QWs separated by 20 nm wide AlGaAsSb lattice matched barriers with 30% Al. A series was grown, were the only variation made was a successive increase of the In-content in the GaInAsSb QW layers from 30% to 48% while keeping the As-content at a fix value of about 7%. This procedure results in a successive increase of the compressive strain in the QW layer sequences.

Figure 17 a) and b) illustrate the 10 K and room temperature photoluminescence spectra, respectively, of three different laser cores comprising five QWs. The three test structures incorporate QW layers all with 6.5% As, whereas the In-content varied between 39 and 48% (39, 43 and 48%). The graph shows clearly that by increasing the In-concentration in the QW layers and thus the compressive strain, the band-to-band PL emission peak shifts at 10 K from 2.29 to longer wavelengths up to 2.47 µm, and similar the room temperature PL emission shifts from 2.54 µm to 2.7 µm. However, the PL intensity decreases monotonously with increasing the lattice mismatch follow by a significant reduction in particular for the third structure (48% In-content) due to the onset of strain relaxation in the laser core layers.

The measured and simulated X-ray diffraction profiles covering the 004-reflection range of the two laser core test structures with In-concentrations of 43 and 48% are displayed in Figure 18. The diffractogram in Figure 18 b) displays the laser core structure containing the highest In-content of 48% in the QWs resulting in a total compressive strain of $17.5 \times 10^{-3}$. The diffraction profile reveals the onset of strain relaxation, as evidenced by slightly broadened SL diffraction peaks and increased background diffraction signal.

The strain of the quantum-well active region is plotted vs. the photoluminescence emission wavelength in Figure 19 for the whole series of test structures. The triangle data represent the laser core series with ternary GaInSb QW active region, and the circles and squares correspond to laser core test structures comprising quaternary GaInAsSb QWs, measured at 10 K and room temperature, respectively. It is clear seen from the graph that the wavelength shifts to longer value upon increasing the strain in the QW layers reaching the longest wavelength of 2.64 µm at room temperature. Notice that for the current series of laser core test structures the active region strain increases steeper with the wavelength as compared to the ternary QW laser core test structures.

## 7. Diode lasers with emission wavelength at 2.4 µm

Based on the above described development of GaInAsSb/AlGaAsSb QW laser core test structure a complete diode laser structure has been grown by MBE, processed using standard optical lithography and CAIBE, and electro-optically characterized. The active region of the diode laser consists of three compressively strained 10 nm thick $Ga_{0.64}In_{0.36}As_{0.10}Sb_{0.90}$ QWs, separated by 20 nm wide $Al_{0.30}Ga_{0.70}As_{0.03}Sb_{0.97}$ lattice matched barriers. The QW active region is imbedded between 400 nm thick $Al_{0.30}Ga_{0.70}As_{0.03}Sb_{0.97}$ SCLs, followed by 2 µm wide n- and p-doped bottom and top cladding layers. Edge emitting Fabry-Perot lasers with 1 mm cavity length have been

realized by facet cleavage. The lasers were In soldered substrate-side down on gold plated copper heat sinks and wire bonded.

Figure 20 depicts the high-resolution lasing emission spectrum of a 3 QW diode laser, revealing well resolved longitudinal modes recorded at 280 K operating temperature. The emission wavelength for the 280 K heat sink temperature is 2.38 µm. The light output power vs injection current characteristic of the present 2.38 µm diode laser, and for comparison the corresponding characteristic of an earlier device emitting at 2.34 µm (laser A in section 2) are displayed in Figure 21. The data was recorded in cw operation mode at 280 K temperature and both devices had a 64 µm x 1000 µm geometry. The 2.34 µm diode laser comprising 30% In and 15% As in the QWs exhibit higher threshold current density of 415 A/cm$^2$ compared to 165 A/cm$^2$ for the 2.38 µm laser structure consisting 36% In and 10% As. This significant decrease in the threshold current density is attributed to a considerable better carrier confinement in particular for the holes in the valence band, see Figure 16. Moreover, higher output power levels exceeding 105 mW have been achieved for the longer wavelength device revealing superior performances as compared to the earlier 2.34 µm diode laser structure.

# II. InAs/GaInSb/AlGaAsSb-based type-II W diode lasers

## 1. Introduction

The material combination InAs/GaInSb/AlGaAsSb offers a variety of possibilities for the realization of type-II diode lasers for the wavelength regime from 3 to 5 µm. Due to the type-II band alignment, the recombining electrons and holes that contribute to the light emission process are localized in different epitaxial layers; therefore the recombination process is spatially indirect. In our structures the band alignment between the various materials combination we use, i.e. InAs, GaInSb and AlGaAsSb, cause the electrons to be localized in the InAs layers and the holes in the GaInSb layers. In contrast to this type-II band alignment, in the type-I configuration used for the diode lasers discussed in the preceding section the recombining electrical carries are confined in the same layer.

Based on the results obtained for the type-I GaInAsSb/AlGaAsSb QW diode lasers, the current project has focused on a second subject being a natural extension of the first part, namely the development of InAs/GaInSb/AlGaAsSb type-II lasers. The type-II QW structures offer a promising approach for the realization of efficient diode lasers for the wavelength interval between 3 and 5 µm. Thus, the development of type-II InAs/GaInSb/AlGaAsSb laser structures offers an excellent extension in terms of emission wavelength to the above-described type-I GaInAsSb/AlGaAsSb QW-lasers. Thus, this part describes the development of InAs/GaInSb/AlGaAsSb type-II laser structures. As for the type-I lasers, the layer sequences of the type-II laser structures were fabricated using also MBE growth on n-type GaSb substrates.

The concept using type-II laser structures offers the possibility to suppress the Auger recombination by proper choice of design parameters, such as thickness of the individual layers, layer composition and concomitant material strain. For the mid-infrared spectral range the Auger process is a major loss mechanism limiting the laser high performances such as maximum cw operating temperature as well as power conversion efficiency, despite excellent material quality achieved by expert growth technique.

## 2. First generation: InAs/GaSb/AlGaAsSb Type-II W-diode lasers

Based on the development of optically pumped W-lasers and W-test-diodes described in the previous final report ["Leucht- und Laserdioden für die optische Kommunikations-technik bei Wellenlängen oberhalb 2 µm", Förderkennzeichen 01 BP 704/9], first electrically pumped W-diode lasers were grown, processed, and electro-optically characterized. The lasers were grown by MBE on n-type (100) GaSb substrates. The W active region comprises 5 periods of InAs/ GaSb/ InAs/ $Al_{0.50}Ga_{0.50}As_ySb_{1-y}$ strain compensated layer sequences, embedded between 400 nm thick $Al_{0.50}Ga_{0.50}As_ySb_{1-y}$ separate confinement layers. The periodical QW layer sequence forming the active region is lattice matched to the GaSb substrate with a relative marginal lattice mismatch of $2{,}7x10^{-3}$. The strain compensation within each of the 5 periods was achieved by

growing the layers with InSb-like interfaces, except for the GaSb on InAs interface. For this interface, the MBE shutter sequence was chosen such as to form a GaAs-like interface. The laser core was sandwiched between 2 µm thick n- and p-doped $Al_{0.85}Ga_{0.15}As_{0.07}Sb_{0.93}$ optical cladding layers, again lattice matched to the GaSb substrate, and GaSb buffer and cap layers. The spatially indirect type-II recombination occurs in this structure between electrons in the conduction band energy states of InAs and holes localized in the valence band energy state of GaSb, as illustrated in Figure 22. Ridge-waveguide Fabry-Perot lasers were prepared by standard photolithography and chemically assisted ion beam etching. Cleaved laser bars were mounted substrate-side down onto copper heat sinks, and attached to the cold finger of a dewar. The lasers were operated in cw mode.

Figure 23 shows the spectral behavior of a 64 µm x 1000 µm device at 77 K, for injection currents below and at threshold. The first two inlays show high resolution Fabry-Perot modes of the electroluminescence (EL), and the third inlay ilustrates the lasing emission at threshold with peak emission wavelength at 3.45 µm. The multiple spectral peaks feature in the electroluminescence are most probably due to substrate modes. Figure 24 displays the high resolved single/double longitudinal modes for different operating temperatures varying between 68 and 77 K for a 64 µm x 1000 µm device. The longitudinal mode spacing at a given injection current amounts to ~1.1 nm. Moreover, by increasing the injection current the wavelength shifts to higher values, resulting in a current tunability of 44 nm/A.

Figure 25 illustrates the cw light output characteristics for a series of operating temperatures from 68 to 80 K, the latter representing the maximum cw lasing temperature for this first generation W-diode laser structure. The cw output power is very low, in the 1 mW regime at liquid nitrogen temperature, and drops rapidly when increasing the operating temperature. The inset shows the corresponding voltage-current characteristics revealing a high turn-on voltage of 1.5 V, severely limiting the device performances. Therefore, to achieve better results this parameter should be improved, i.e. values below 1 V would be desirable. The temperature sensitivity of the threshold current is shown in Figure 26, revealing a characteristic temperature of 23 K, significantly lower as compared to the value achieved by the NRL group of 38 K, however for a different active region design [W. W. Bewley et al., Appl. Phys. Lett. 76, 256 (2000)].

## 3. New design: InAs/GaInSb/AlGaAsSb type-II interband bound-to-miniband superlattice lasers

*Design*

Following the results obtained for our first generation electrically pumped W-lasers we have concentrated our efforts towards further development of the electrically injection type-II InAs/GaInSb/AlGaAsSb W lasers. First, we have focused on a new design of the W-configuration; a new W region was created insuring improved electrical injection into the active region. The design involves the use of a superlattice (SL) layer sequence active region comprising a periodical sequence of four constituent layers, all with thickness of

just a few monolayers, including thin interperiod barriers. However, the periodicity is different for electrons and holes: for the electrons the period is effectively a two layer sequence as the barrier heights generated by the GaInSb and AlGaAsSb are almost the same, while for the holes a four layer sequence, like the nominal growth period, resulting in miniband states in the conduction band and localized states in the valence band. Thus, the electrons are delocalized over the active region due to their 3 dimensional density of state (DOS) whereas the holes are localized with a 2 dimensional density of state. Therefore, the use of superlattice rather than multiple quantum well structure results in a significantly improved electronic transport representing a notable advantage of the new design. Moreover, as compared to pure InAs/GaInSb SL structure, our new design has the advantage of a stronger interband matrix element and thus a stronger stimulated emission due to the 2 dimensional density of states for the holes, while the previous SL structure has a 3 dimensional DOS for both electrons and holes as well. One period of the new W-sequence consist of the light emitting three constituents InAs/GaInSb/InAs layer sequence separated by lattice matched AlGaAsSb interperiod barriers with low Al-content. In this design the spatially indirect type-II recombination occurs between electrons in the miniband states of the conduction band and holes in the valence band states of GaInSb, as schematically shown in Figure 27. The spatial distribution of the valence and conduction band edge, the position of the quantization energy levels and miniband as well as the probability functions for the electrons and holes are illustrated in Figure 27.

*Superlattice laser core test structures*

The concept phase was followed by growth of laser core test layer sequence for type-II SL lasers using a conventional solid source MBE growth system and right away accompanied by on wafer level characterization performed by ex-situ PL and XRD analysis. SL laser core test layers have been grown on GaSb substrates incorporating 10 W periods. An important aspect in the laser development is the optimization of MBE growth parameters. For this purpose, using the above described design we have focused on the growth optimization by establishing the most favorable core growth temperature, varying between 380°C and 460°C in steps of 20°C. Additional variations included the interface (IF) bonds formation, by using two kinds of shutter sequences, alternating (A) and alternating with continuous group V stabilization (AC). The former shutter sequence gives rise to truly alternating GaAs-like and InSb-like IF bonds, while the latter leads to effectively mixed IF bonds.

Several SL laser core test structures grown at different temperatures have been optically characterized. A Nd:YAG laser (1064 nm) has been used as excitation source for the PL spectroscopy. The W-laser cores exhibited relatively intense band to band luminescence centered at wavelengths of 3.36 and 3.39 µm, respectively. The best results in terms of PL intensity yielded the 420°C core growth temperature, thus being the optimum value in the 380 to 460°C temperature range. Therefore, this growth temperature has been used for growth of the active region throughout the subsequent SL W-laser growth series.

Figure 28 illustrates a high resolution X-ray diffraction profile of an InAs/GaInSb/InAs/AlGaAsSb SL laser core test structure with a 420°C core growth temperature consisting mixed interface sequences. The zero order superlattice (SL) peak

is shifted to just marginally smaller diffraction angle as compared to the GaSb 004 substrate reflection, corresponding to a minor latticed mismatch of $((d_{SL}-d_{GaSb})/d_{GaSb})_{\perp} = 5.6x10^{-3}$. This excellent lattice matching is achieved mainly due to the formation of net zero strain IF sequences. Measurements covering a wide angle range from 25° to 35° show SL reflections up to the 7th order, which leads us to conclude that an excellent structural quality of the structure was achieved.

*Superlattice bound-to-miniband diode lasers*

After optimizing the growth of the SL laser core test structure we headed towards the SL diode laser itself. The laser structures incorporate type-II InAs/GaInSb/InAs/AlGaAsSb SL layer sequences, imbedded between two 0.6 µm thick AlGaAsSb separate confinement layers (SCL) forming the core of the optical waveguide. 1.5 µm thick n- and p-type $Al_{0.85}Ga_{0.15}As_{0.07}Sb_{0.93}$, lattice matched to the GaSb substrate, have been used as optical cladding layers. Several laser structures have been grown varying the upper cladding growth temperature between 470 to 530°C, the interface bonds and the number of W-periods, 5 and 10. Again, following growth the epitaxial layer structures were analyzed by PL, HRXRD and SIMS in order to determine the precise PL emission wavelength and profile, the strain and individual layer compositions, as well as the doping concentrations. The entire layer sequence was grown by MBE on n-GaSb substrate and processed in ridge waveguide diode lasers using optical lithography and CAIBE.

Figure 29 shows the photoluminescence spectra for three SL diode laser structures recorded at 77 K with different upper cladding growth temperature, 530, 500 and 470°C. All three devices consisted a 5-period SL. The peak emission wavelength of these laser structures is between 3.18 and 3.27 µm, shifting to longer wavelengths with increasing upper cladding growth temperature. The SL diode laser with the 530°C upper cladding growth temperature exhibited a 25% higher PL intensity as compared to the other two laser structures. This result match well the fact that Al-containing epitaxial layers should be grown at high temperatures in order to achieve superior material quality.

Figure 30 displays the emission spectra in cw mode at different heat sink temperatures including the cw maximum operating temperature of 185 K, for a 64 µm x 1000 µm laser diode consisting 10 periods with mixed interfaces and upper cladding growth temperature of 500°C. The laser output contains multiple longitudinal modes, and the peak lasing wavelength shifts from 3.166 µm at 90 K to 3.255 µm at 185 K resulting in a temperature tunnability of ~ 0.9 nm/K. The emission wavelength bandwidth is contained within ~ 15 nm. However, at most temperatures the emission spectrum exhibit two maximum separated by about 30 nm. Similar spectral behavior has been observed by Meyer et al. for multiple-quantum-well W-diode lasers [W. W. Bewley et al., Appl. Phys. Lett. 76, 256 (2000)].

CW light-current characteristics recorded at a series of operating temperature between 90-185 K are shown in Figure 31. The 10-period structure shows lasing up to 185 K under cw conditions, while the 5-period device up to a slightly lower temperature of 177 K. At 110 K a maximum output power of 59 mW per facet has been obtained limited by thermal rollover. The inset illustrates the corresponding current-voltage

characteristic for the various temperatures in the 90-185 K range. The diode lasers exhibited superior electrical properties as compared to the first generation reflected by relatively low turn-on voltages varying between 0.9 and 1.1 V in the measured temperature interval. Moreover, the differential resistance is as low as ~ 200 mΩ at 0.5 A. CW differential quantum efficiency ($\eta_d$) of 28% (61 mW/A) for the 5-period device and slightly lower 22% (41 mW/A) for the 10-period laser structure have been obtained at 110 K operating temperature.

The temperature dependence of the threshold current for a 10-period laser structure comprising mixed interfaces and 500°C upper cladding growth temperature is shown in Figure 32. A relatively high characteristic temperature of 100 K is achieved for the low temperature range, representing a major improvement as compared to the 23 K value obtained for our first generation W-lasers. However, a considerable drop in $T_0$ is observed amounting to 33 K for operating temperatures above 140 K. Regardless, both values compare favorably well to the $T_0$ = 38 K reported by the NRL group for a multiple-quantum-well W-diode laser [W. W. Bewley et al., Appl. Phys. Lett. 76, 256 (2000)].

To improve the laser performances in terms of output power, the rear facet of a 1000 µm long laser bar was high-reflectivity coated (HR-95%) using alternating Si and $SiO_2$ double-layers, while the front facet was anti-reflection coated (AR-5%) by a SiN layer. Figure 33 shows the light-current characteristics at 110 K of a 64 µm x 1000 µm laser bar in cw mode with uncoated facets (dash-doted curve) and with HR/AR coated facets (solid curve), and in pulsed operation with HR/AR facets (dashed curve). The diode lasers were mounted substrate side down, limiting the maximum achievable cw output due to thermal rollover. CW output power in the linear regime of 66 mW was achieved for the coated laser in comparison with 44 mW/facet without coating at the same drive current (1.2 (A)). In cw operation the coated devices show saturation behavior in the P-I characteristic at a current level of 1.5 A and thermal rollover at around 2.3 A, limiting the maximum available cw output power at 100 mW. This limitation in the output power can be ascribed to the heating of the device because of the substrate-side down mounting. In fact, mounting of the laser bars junction-side down is expected to improve considerably the P-I characteristics and the maximum available output power due to the improved thermal coupling of the junction to the heat sink. To overcome saturation in the output power caused by the limited heat transfer from the active region to the heat sink, pulsed P-I measurements with 5 µs pulse width and 5% duty cycle were performed on the HR/AR coated laser. Peak output powers in excess of 132 mW were achieved without reaching thermal rollover. This result demonstrates the potential of the present 3.2 µm type-II InAs/GaInSb/InAs/AlGaAsSb SL bound-to-miniband laser diodes.

In addition, short pulse measurements have been performed for a 10-period diode laser using short current pulses of 100 ns and repetition rate of 5 kHz. A maximum pulsed operating temperature up to 260K has been demonstrated.

# III. Subcontract

Supplementary to the above described approach of MBE growth of GaSb-based structures, an alternative growth of III-antimony structures in general, and (GaIn)(AsNSb) QWs on GaAs in particular, using MOCVD was investigated by Prof. Dan Fekete at the Technion in Haifa (Israel). This work was performed in the frame of a subcontract. The final report of the project partner documenting the achieved developments related with MOCVD growth of III-Antimonides is enclosed in this bulletin.

# IV. Summary

The aim of the current project was the development of diode lasers for the wavelength range above 2 µm based on the III-V antimonide semiconductor material system. Electrically pumped lasers for the 1.7 to 2.34 µm wavelength interval have been realized, with active region comprising GaInAsSb type-I QW layers separated by AlGaAsSb barriers, and embedded between cladding layers forming the optical waveguide. By varying the In and As composition in the QWs a set of ten diode lasers have been fabricated with emission wavelength covering the 1.7 to 2.34 µm spectral range. High characteristic temperature of 179 K has been achieved for diode lasers emitting at 1.94 µm, however $T_O$ decreases from 179 K to 54 K when proceeding from the short wavelength device (1.94 µm) to the longest wavelength of 2.34 µm. In order to understand the decrease of $T_O$ with increasing wavelength, we have analyzed the two main contributions responsible for the temperature sensitivity of $I_{th}$, explicitly the Auger recombination and the heterobarrier carrier leakage. Our experimental results led us to conclude that of the two loss mechanisms, the temperature dependence of $I_{th}$ is governed by thermally activated heterobarrier carrier leakage, limiting the high-temperature performances of the present mid-infrared diode lasers.

Furthermore, the beam quality of these laser structures has been studied by analyzing the far field (FF) distribution both along the slow axis and fast axis. The measurements were performed on diode lasers with 16 µm x 1000 µm geometry and HR/AR coated facets at room temperature. The measured fast axis profiles exhibited a Gaussian shape with full-width at half-maximum (FWHM) divergence angle of ~ 67°, which compared well with the calculated value of 60°. In contrast to the transversal pattern, however, the lateral FF showed multiple-mode behavior. Upon increasing the injection current, the profile shape changed, showing higher order side peaks, and the FWHM of the divergence angle increased slightly from 4.8° ($2I_{th}$) to 5.6° ($4I_{th}$). The angular position of the measured side peaks originating from higher order modes was in excellent agreement with the calculations.

Further on, the heterobarrier leakage due to thermally activated carriers has been investigated in detail. By increasing the Al concentration in the barriers and SCLs, a higher band offset in both the conduction and valence band is formed leading to a better carrier confinement and to a suppressed heterobarrier carrier leakage. For this study, a series of three diode lasers designed for 2.23 µm emission wavelength with three QWs were grown, varying the Al-composition (20%, 30% and 40%) in the barriers and SCLs. The light-current characteristics at 280 K revealed comparable threshold currents for the 20% and 30% Al-content lasers, however a considerable increase by about a factor of two is obtained for the 40% Al laser. This significant increase of $I_{th}$ may be attributed to the crossover of the $\Gamma$ and L conduction bands minima with the X minima, which occurs at Al compositions of around 40% in ternary AlGaSb alloys. Regarding power efficiency, out of the three laser structures, the device with the lowest Al-composition of 20% revealed the highest power efficiency over the whole injection current range. Moreover, a maximum value of 30% is achieved for this laser structure, representing a record high value for 2.23 µm emission wavelength.

A high characteristic temperature $T_O$ = 93 K is achieved for the 40% Al-content device in the complete temperature range, while for the lower Al-content devices two

distinctive regimes are observable, yielding lower $T_O$ values above 310 K. We found that for the high temperature range (250 - 360 K), the device with 40% Al-content had a major advantage regarding $T_O$ as compared to those with 20% and 30% Al-content, with $T_O$ values of 63 and 66 K, respectively. The high $T_O$ is associated with a better carrier confinement, leading to reduced heterobarrier leakage losses in the laser structure. In conclusion, the high $T_O$ value correlates with the increased band offsets in both the conduction ($\Delta E_C$) and valence bands ($\Delta E_V$).

In an attempt to extend the emission wavelength towards 2.7 µm, we first have focused on the development of laser core test structure. The concept we adopted to achieve longer lasing wavelength was: increase the In-content in the QWs while keeping the As-concentration at a constant value until the strain relaxation begins. As next, set the As-content to a higher value and over again successively increase the In-content in the QWs till strain relaxation occurs. The emission wavelength is determined by the In- and As-concentration in the QWs, however, there is a trade-off between longer wavelength and week carrier confinement due to small band offsets in particular in the valence band. Thus, the approach is increase the In-content and keep the As concentration low as possible to prevent strain relaxation. Following the above-described iteration, laser core test structure with room temperature PL emission at 2.64 µm has been demonstrated, consisting of GaInAsSb compressively strained QW layers with 48% In and about 7% As. Based on this achievement, a complete diode laser structure has been grown using three compressively strained $Ga_{0.64}In_{0.36}As_{0.10}Sb_{0.90}$ QWs, separated by $Al_{0.30}Ga_{0.70}As_{0.03}Sb_{0.97}$ lattice matched barriers. Lasing emission at 2.38 µm has been demonstrated at 280 K operating temperature, exhibiting light output powers beyond 105 mW.

In the frame of the present project, as a second subject longer wavelength mid-infrared lasers have been studied. Electrically pumped type-II InAs/GaInSb/AlGaAsSb W-lasers have been realized, targeting emission wavelengths between 3 and 5 µm. The first design included InAs/GaSb/InAs/AlGaAsSb W-active regions with 50% Al, and an emission wavelength of around 3.5 µm has been demonstrated. However, these devices exhibited a poor performance, operating just up to 80 K in cw mode, and emitting light output powers in the sub mW regime. The characteristic temperature was low as well, 23 K, compared to 38 K reported in the literature for similar laser structures. Based on the results obtained from this first design, a new design has been realized, including lower Al concentrations in the barriers and SCLs, for improved carrier injection, as well as the use of SL structure instead of "W" multiple QWs for enhanced electrical transport. Indeed, this second generation W-diode lasers exhibited a significantly improved electro-optical performance compared to the first generation W-diode lasers.

Firstly, in search of the optimal upper cladding growth temperature, the SL diode laser with 530°C upper cladding growth temperature exhibited the highest PL intensity as compared to the other laser structures grown with lower upper cladding temperatures of 500 and 470°C. However, no wonder due to the fact that Al-containing epitaxial layers should be grown at high temperatures for realizing excellent material quality. The diode lasers exhibited superior electrical properties reflected by relatively low turn-on voltages varying between 0.9 and 1.1 V in the 90 - 185 K temperature interval. Furthermore, the cw emission spectra contained multiple longitudinal modes and for most devices the laser output exhibited two maximum separated by about 30 nm,

behavior that has been reported also by Meyer et al. [W. W. Bewley et al., Appl. Phys. Lett. 76, 256 (2000)]. Regarding the temperature tunnability of the emission wavelength, for example a 10-period laser structure comprising mixed interfaces and upper cladding growth temperature of 500°C revealed lasing wavelength shift from 3.166 µm at 90 K to 3.255 µm at 185 K, leading to a slope of ~ 0.9 nm/K. Concerning maximum operating temperature, the 10-period structure showed lasing up to 185 K, under cw conditions, while the 5-period device showed lasing up to a slightly lower temperature of 177 K. Moreover, using short current pulses of 100 ns and repetition rate of 5 kHz, a maximum pulsed operating temperature of 260 K could be demonstrated for a 10-period diode laser.

Output powers of 59 mW per facet have been obtained at 110 K limited by thermal rollover. Further, cw differential quantum efficiency ($\eta_d$) of 28% (61 mW/A) for the 5-period device and slightly lower 22% (41 mW/A) for the 10-period laser structure have been obtained at 110 K operating temperature. Significantly improvement in the output power has been achieved by applying high-reflectivity (HR-95%) and anti-reflection (AR-5%) coatings to the mirror facets. Light output of 100 mW in cw mode has been demonstrated for diode lasers mounted substrate side down, however the maximum achievable output power was limited by the thermal rollover onset. To overcome this saturation in the output power pulsed P-I measurements with 5 µs pulse width and 5% duty cycle were performed on the HR/AR coated laser. Peak output powers in excess of 132 mW were achieved without reaching thermal rollover.

Additionally, characteristic temperatures of 100 K have been demonstrated for the low temperature interval representing a major improvement as compared to the 23 K value obtained for our first generation W-lasers. However, for the high temperature regime a modest value of just 33 K has been deduced. Regardless, both values compare favorably well to the $T_0$ = 38 K reported by the NRL group for a multiple-quantum-well W-diode laser. All the above-achieved results demonstrate the potential of the present 3.2 µm type-II InAs/GaInSb/InAs/AlGaAsSb SL bound-to-miniband laser diodes.

# V. Conclusions

The current project was successful in establishing the material and technology basis for mid infrared ($\lambda > 2$ µm) semiconductor QW diode lasers on the basis of the (AlGaIn)(AsSb) material combination.

Highly efficient type-I diode lasers for the emission wavelength between 1.7 and 2.4 µm have been realized; this development was the starting point for two further BMBF funded research projects ("Leistungsdiodenlaser mit Emissionswellenlängen von 2 µm für die Medizintechnik und die Materialbearbeitung", Förderkennzeichen 13N8236, and "Erarbeitung GaSb-basierender Rippenwellenleiter-Diodenlaser hoher Effizienz und Strahlqualität", Förderkennzeichen 13N8491).

Further, successful design has been implemented for the realization of type-II InAs/GaInSb/AlGaAsSb W-lasers for emission wavelength $\lambda > 3$ µm. The diode lasers based on our proposed design exhibited enhanced performances as compared to similar laser structures reported in the literature with emission wavelength around 3.2 µm. Moreover, we applied for a patent with our design (C. Mermelstein, J. Wagner and J. Schmitz, "Interband bound-to-miniband superlattice laser", Deutsche Patentanmeldung Amtsaktenzeichen 103 53 389.3, patent filed on 14.11.03).

Complementary to the approach of MBE growth of GaSb-based structures, an alternative growth technique for III-antimony structures in general, and (GaIn)(AsNSb) QWs on GaAs in particular, namely MOCVD was investigated by Prof. Dan Fekete at the Technion in Haifa (Israel). This work was performed in the frame of a subcontract. Regarding the growth of GaSb-based structures, the MOCVD technique indeed is more complex as compared to the MBE growth, in addition to the fact that the partner had a very ambitious goal namely to grow quinternary GaInAsNSb epitaxial layers, whereas already the growth of quaternary GaInAsSb without the incorporation of N is enough challenging. Regarding the growth of GaInAsNSb QW layers, Prof. Fekete got to the conclusion that "using MOCVD it is impossible to grow QWs with the desired composition". To circumvent this problem an alternative approach, namely replacing the quinternary GaInAsNSb QWs by GaInAs/GaAsNSb ternary/quaternary QW layers has been explored. In summary, the achievements of Prof. Fekete are valuable in particular in terms of theory, calculation and modeling. For details regarding his contribution to the project see separate final report included in this bulletin. Therefore, we conclude that the MBE is the state of the art growth method for GaSb-based semiconductor structures, and so far represents the growth technique of choice to produce high epitaxial material quality.

A general trend to longer wavelengths is observed in optical free space communication. The 3-5 µm wavelength range has the advantage of considerably reduced losses due to scattering from fog, mist and dust as compared to the near-infrared commercial existing systems using the 850 nm and 1.55 µm laser sources. Thus, the type-II W-lasers are an attractive laser light source for this spectral window.

Below are listed several references related to commercially available FSO communication system using 850 nm and 1.55 µm diode lasers sources, followed by references regarding the implementation of longer wavelength semiconductor lasers:

1. I. I. Kim, R. Stieger, J. Koontz, C. Moursund, M. Barclay, P. Adhikari, J. Schuster, and E. Korevaar, *"Wireless optical transmission of fast ethernet, FDDI, ATM, and ESCON protocol data using the TerraLink laser communication system"*, Opt. Eng. 37, 3143–3155 (1998).

2. I. I. Kim, B. McArthur, and E. Korevaar, *"Comparison of laser beam propagation at 785 nm and 1550 nm in fog and haze for optical wireless communications"*, in Optical Wireless Communications III*,* E. J. Korevaar, ed., Proc. SPIE 4214, 26–37 (2001).

3. P. F. Sajowski, G. Nykolak, J. J. Auburn, H. M. Presby, G. E. Tourgee, E. Korevaar, J. Schuster, and I. I. Kim, *"2.4 km Free-Space Optical Communication 1550 nm Transmission Link Operating at 2.5 Gb/s – Experimental Results"* in Optical Wireless Communications, 1998, E. J. Korevaar, ed., Proc. SPIE 3552, pp. 29 – 40.

4. M. Fuller, "City carriers beam in with wireless optics", Fibre System, June 2000.

5. "Optical wireless beams in on the last-mile markets", Fibre System Europe, January 2001.

6. "Free-space lasers solve the last-mile bottleneck", Opto & Laser Europe, March 2001.

7. H. A. Willerbrand, B.S.Ghuman, "Fiber optics without fiber", IEEE Spectrum, August 2001.

8. "Free-space optics 'available' for the last mile?", LIGHTWAVE, July 2000.

New generation demonstrators based on long-wavelength ($\lambda$ >10 µm) quantum cascade lasers (QCL) were demonstrated by the group of J. Faist from Uni. Neuchatel (CH) and the group of Capasso at Lucent Technologies, Bell Labs Innovations (USA)

9. J. Faist, D. Hofstetter, M. Beck, T. Aellen, M. Rochat, and S. Blaser, "*Bound-to-continuum and two-phonon resonance quantum cascade lasers for high duty cycle, high temperature operation*", IEEE J. Quantum Electron. 38, 533 (2002).

10. F. Capasso, R. Paiella, R. Martini, R. Colombelli, C. Gmachl, T. L. Myers, M. S. Taubman, R. M. Williams, C. G. Bethea, K. Unterrainer, H. Y. Hwang, D. L. Sivco, A. Y. Cho, A. M. Sergent, H. C. Liu, and E. A. Whittaker, *"Quantum cascade lasers: ultrahigh-speed operation, optical wireless communication, narrow linewidth, and far-infrared emission"*, *IEEE J. Quantum Electron.* 38, 511 (2002).

11. R. Martini, R. Paiella, C. Gmachl, F. Capasso, E.A. Whittaker, H.C. Liu, H.Y. Hwang, D.L. Sivco, J.N. Baillargeon, A.Y. Cho, "*High-speed digital data transmission using mid-infrared quantum cascade lasers*", Electron. Lett. 37, 1290 (2001).

Additionally, recent information on the topic is presented in the December 2003 issue of Laser Focus World, *"Free-space optics builds invisible bridges"* by K. Kincade.

# VI. Publications and Presentations

## 1. Publications


**1.** S. Simanowski, C. Mermelstein, M. Walther, N. Herres, R. Kiefer, M. Rattunde, J. Schmitz, J. Wagner, and G. Weimann, *"Growth and layer structure optimization of 2.26 µm (AlGaIn)(AsSb) diode lasers for room-temperature operation",* Proc. of the 11th International Conference on Molecular Beam Epitaxy (2000).

**2.** M. Rattunde, C. Mermelstein, S. Simanowski, J. Schmitz, R. Kiefer, F. Fuchs, M. Walther, and J. Wagner, *"Temperature dependence of threshold current for 1.8 to 2.3 µm (AlGaIn)(AsSb)-based QW diode lasers",* Proc. 27th International Symposium on Compound Semiconductors (2000).

**3.** M. Rattunde, C. Mermelstein, S. Simanowski, J. Schmitz, R. Kiefer, N. Herres, F. Fuchs, M. Walther, and J. Wagner, *"(AlGaIn)(AsSb)-based QW diode lasers for the 1.8 to 2.3 µm wavelength range",* Digest of the 2001 Conference on Mid-Infrared Optoelectronics Materials and Devices (MIOMD 2001), 40 (2001).

**4.** M. Rattunde, C. Mermelstein, S. Simanowski, J. Schmitz, R. Kiefer, N. Herres, F. Fuchs, M. Walther, and J. Wagner, "*Temperature dependence of threshold current for 1.8 to 2.3 µm (AlGAIn)(AsSb)-based QW diode lasers"*, in Proc. of the 27th Int. Symp. on Compound Semiconductors, Institute of Electrical and Electronics Engineers, Inc., USA, p. 437 (2001).

**5.** S. Simanowski, C. Mermelstein, M. Walther, N. Herres, R. Kiefer, M. Rattunde, J. Schmitz, J. Wagner, and G. Weimann, *"Growth and layer structure optimization of 2.26 µm (AlGaIn)(AsSb) diode lasers for room-temperature operation",* J. of Crystal Growth 227-228, 595 (2001).

**6.** J. Wagner, M. Rattunde, C. Mermelstein, J. Schmitz, R. Kiefer, F. Fuchs, and M. Walther, "*Group III-antimonides: material basis for diode lasers emitting at wavelengths beyond 2 µm",* in Proc. of the "Materials Week 2001", Int. Congress on Advanced Materials and Processes, Munich, (2001).

**7.** C. Mermelstein, M. Rattunde, J. Schmitz, S. Simanowski, R. Kiefer, M. Walther, and J. Wagner, *"Sb-based mid-infrared diode lasers"*, Proc. 2001 MRS Fall Meeting.

**8.** C. Mermelstein, M. Rattunde, J. Schmitz, R. Kiefer, M. Walther, and J. Wagner, *"Physics and applications of III-Sb based type-I QW diode lasers"*, Proc. SPIE 4651, 173 (2002).

**9.** M. Rattunde, C. Mermelstein, J. Schmitz, R. Kiefer, W. Pletschen, M. Walther, and J. Wagner, *"Comprehensive modeling of the electro-optical-thermal behavior of (AlGaIn)(AsSb)-based 2.0 µm diode lasers",* Appl. Phys. Lett. 80, 4085 (2002).

**10.** M. Rattunde, C. Mermelstein, J. Schmitz, R. Kiefer, W. Pletschen, M. Walther, and J. Wagner, *"GaSb-based diode lasers for power applications in the 2 to 2.3 µm spectral range",* Proc. MIOMD-V 5th Int. Conf. On Mid-IR Optoelectronic Materials and Devices, p. 177 (2002).

**11.** M. Rattunde, C. Mermelstein, J. Schmitz, R. Kiefer, W. Pletschen, M. Walther, and J. Wagner, *"Temperature sensitivity of high power GaSb based 2 µm diode lasers",* in Proc. of the 29th Int. Symp. on Compound Semiconductors, Bristol, Philadelphia: IOP Publishing 2003 IOP Conference Series 174, 347 (2003).

**12.** C. Mermelstein, J. Schmitz, R. Kiefer, M. Walther, and J. Wagner, *"Type-II W-laser based on III-arsenide/antimonides"*, in Proc. 33. IR Kolloquium, (2003).

**13.** M. Rattunde, C. Mermelstein, J. Schmitz, R. Kiefer, W. Pletschen, M. Walther, J. Wagner, *"GaSb-based diode lasers for power applications in the 2 µm spectral range"*, in Proc. of the Conference on Lasers and Electro-Optics/Europe (CLEO/Europe) (2003).

## 2. Presentations

**1.** S. Simanowski, C. Mermelstein**,** M. Walther, N. Herres, R. Kiefer, M. Rattunde, J. Schmitz, J. Wagner, and G. Weimann, *"Growth and layer structure optimization of 2.26 µm (AlGaIn)(AsSb) diode lasers for room-temperature operation",* 11th Int. Conference on Molecular Beam Epitaxy, Beijing (China), 10. - 15.9.00

**2.** M. Rattunde, C. Mermelstein, S. Simanowski, J. Schmitz, R. Kiefer, F. Fuchs, M. Walther, and J. Wagner, *"Temperature performance of (AlGaIn)(AsSb)-based QW diode lasers for the 1.8 to 2.3 µm wavelength range",* 27th Int. Symposium on Compound Semiconductors (ISCS 2000), Monterey, CA (USA), 2. - 5.10.00

**3.** J. Schmitz, F. Fuchs, N. Herres, C. Mermelstein, M. Walther, *"MBE Growth of InAs/GaSb/AlSb based Type II Quantum-Well Lasers"*, 11th European Workshop on Molecular Beam Epitaxy, Hinterzarten (Germany), 4.-7.02.2001

**4.** J. Schmitz, F. Fuchs, N. Herres, C. Mermelstein, M. Walther, *"MBE Growth of InAs/(GaIn)Sb/AlSb based Infrared Lasers and Detectors"*, French-German Crystal Growth Meeting, Seeheim Jugenheim (Germany), 6.-7.03.2001

**5.** M. Rattunde, C. Mermelstein, S. Simanowski, J. Schmitz, R. Kiefer, N. Herres, F. Fuchs, M. Walther, and J. Wagner, *"(AlGaIN)AsSb)-based QW diode lasers for the 1.7 to 2.3 µm wavelength range",* Conference on Mid-Infrared Optoelectronics Materials and Devices (MIOMD 2001), Montpellier (France), 1.-4.04.2001

**6.** M. Rattunde, C. Mermelstein, S. Simanowski, J. Schmitz, R. Kiefer, W. Pletschen, N. Herres, F. Fuchs, M. Walther, and J. Wagner, "*Antimonidische 2µm-Diodenlaser für Spektroskopie und Leistungsanwendungen*", 31. IR Kolloquium, IAF Freiburg, 25-26.4.2001

**7.** C. Mermelstein, J. Schmitz, F. Fuchs, Q. Yang, R. Kiefer, and J. Wagner, "InAs/GaSb/AlGaAsSb type-II W-Diode Lasers", 31. IR Kolloquium, IAF Freiburg, 25-26.4.2001

**8.** J. Wagner, M. Rattunde, C. Mermelstein, J. Schmitz, R. Kiefer, F. Fuchs, and M. Walther, "*Group III-antimonides: material basis for diode lasers emitting at wavelengths beyond 2 µm",* Materials Week 2001, Int. Congress on Advanced Materials and Processes, Munich (Germany) 1.-4.10.2001

**9.** C. Mermelstein, *"III-V semiconductor quantum-well diode lasers for the 2-5 µm spectral range"*, Seminar Talk, Kyushu Institute of Technology, Kitakyushu (Japan), 9.11.2001

**10.** M. Rattunde, C. Mermelstein, J. Schmitz, R. Kiefer, W. Pletschen, F. Fuchs, M. Walther, J. Wagner, *"Power efficiency of GaSb based 2.0 µm diode lasers*" LEOS 2001 / IEEE LEOS Annual Meeting, San Diego, CA (USA), 12.-15.11.2001

**11.** C. Mermelstein, M. Rattunde, J. Schmitz, S. Simanowski, R. Kiefer, M. Walther, and J. Wagner, *"Sb-based mid-infrared diode lasers"*, 2001 MRS Fall Meeting, Symposium H: "Progress in Semiconductor Materials for Optoelectronic Applications", Invited Talk, Boston, MA (USA), 26. – 30.11.2001

**12.** C. Mermelstein, *"III-V semiconductor quantum-well diode lasers for the 2-5 µm spectral range"*, Seminar Talk, David Sarnoff Research Center, Princeton, NJ (USA), 3.12.2001

**13.** C. Mermelstein, *"III-V semiconductor diode lasers for the mid-infrared"*, Seminar Talk, University Freiburg, (Germany), 14.12.2001

**14.** C. Mermelstein, *"III-V semiconductor diode lasers for the mid-infrared"*, Seminar Talk, Fraunhofer Institute IPM Freiburg, (Germany), 16.01.2002.

**15.** C. Mermelstein, M. Rattunde, J. Schmitz, R. Kiefer, M. Walther, and J. Wagner, *"Physics and applications of III-Sb based type-I QW diode lasers"*, Invited talk, SPIE Photonics West 2002, San Jose, CA (USA), 20-25.01.2002

**16.** C. Mermelstein, *"III-Sb semiconductor diode lasers for the mid-infrared"*, University of Iowa, Iowa City, IA (USA), 29.01.2002

**17.** M. Rattunde, C. Mermelstein, J. Schmitz, R. Kiefer, W. Pletschen, M. Walther, and J. Wagner "Antimonidische 2µm-Diodenlaser für Leistungsanwendungen: Status und Anwendungen" 32. IR-Kolloquium, Freiburg (Germany), 23-24 April 2002

**18.** M. Rattunde, C. Mermelstein, J. Schmitz, R. Kiefer, W. Pletschen, M. Walther, and J. Wagner, *"GaSb-based diode lasers for power applications in the 2 to 2.3 µm spectral range",* 5th Int. Conf. On Mid-Infrared Optoelectronic Materials and Devices (MIOMD-V), Annapolis, MD (USA), 8-11 September 2002.

**19.** C. Mermelstein, *"Group III-Antimonide Based Type-I QW Diode Lasers"*, Naval Research Laboratory, Washington DC (USA), 13 September 2002

**20.** M. Rattunde, C. Mermelstein, J. Schmitz, R. Kiefer, W. Pletschen, M. Walther, and J. Wagner, *"Temperature sensitivity of high power GaSb based 2 µm diode lasers",* 29th International Symposium on Compound Semiconductors (ISCS 2002), Lausanne (Switzerland), 7-10 October 2002.

**21.** J. Schmitz, C. Mermelstein, M. Rattunde, R. Kiefer, M. Walther, and J. Wagner, *"Antimonidische Laser bei 2 µm"*, German MBE-Workshop 2002, Freiburg (Germany), 21-22 October 2002

**22.** C. Mermelstein, *"Mid-Infrared Semiconductor QW Diode Lasers"*, Department of Electrical Engineering, Tel Aviv University, Tel Aviv (Israel), 28 October 2002

**23.** C. Mermelstein, *"Mid-Infrared Semiconductor Diode Lasers at Fraunhofer-IAF"*, Glucon Medical Ltd., Petach-Tikva, (Israel), 13 January 2003.

**24.** C. Mermelstein, *"Mid-Infrared Semiconductor QW Diode Lasers"*, Department of Electrical Engineering, Stanford University, Stanford, CA (USA), 31 January 2003.

**25.** J. Schmitz, C. Mermelstein, M. Rattunde, F. Fuchs, R. Kiefer, M. Walther, and J. Wagner *"MBE Growth of Sb-based Infrared Lasers and Detectors"* 12th Euro-MBE Workshop, Bad Hofgastein (Austria), 16.-19. February 2003.

**26.** C. Mermelstein, J. Schmitz, R. Kiefer, M. Walther, and J. Wagner, *"Type-II W-laser based on III-arsenide/antimonides"*, 33. IR Kolloquium, Freiburg (Germany), 8.-9. April 2003.

**27.** C. Mermelstein, *"Mid-Infrared Semiconductor QW Diode Lasers"*, Soreq Nuclear Research Center, Yavne, Israel, 30 April 2003.

**28.** M. Rattunde, C. Mermelstein, J. Schmitz, R. Kiefer, W. Pletschen, M. Walther, and J. Wagner, *"GaSb-based diode lasers for power applications in the 2 µm spectral range"*, Conference on Lasers and Electro-Optics/Europe (CLEO-Europe), Munich (Germany) 22.-27. June 2003.

**29.** C. Mermelstein, J. Schmitz, R. Kiefer, M. Walther, and J. Wagner, *"InAs/GaInSb/ AlGaAsSb based type-II W-lasers"*, 30th Int. Symp. on Compound Semicond. (ISCS 2003), San-Diego, CA (USA), 25.-27. August 2003.

## 3. Patent application

C. Mermelstein, J. Wagner and J. Schmitz, "Interband bound-to-miniband superlattice laser", Deutsche Patentanmeldung, Amtsaktenzeichen 103 53 389.3, patent filed on 14.11.03

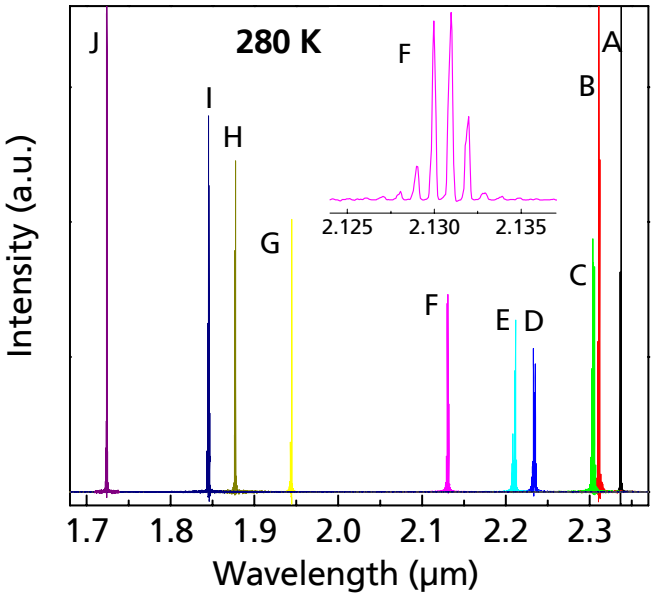


**Fig. 1** 280 K lasing spectra of ten different diode lasers covering the wavelength interval from 1.7 to 2.34 μm. The inset displays the emission of the 2.13 μm diode laser on an expanded wavelength scale. All lasers had a 64 μm x 600 μm geometry.

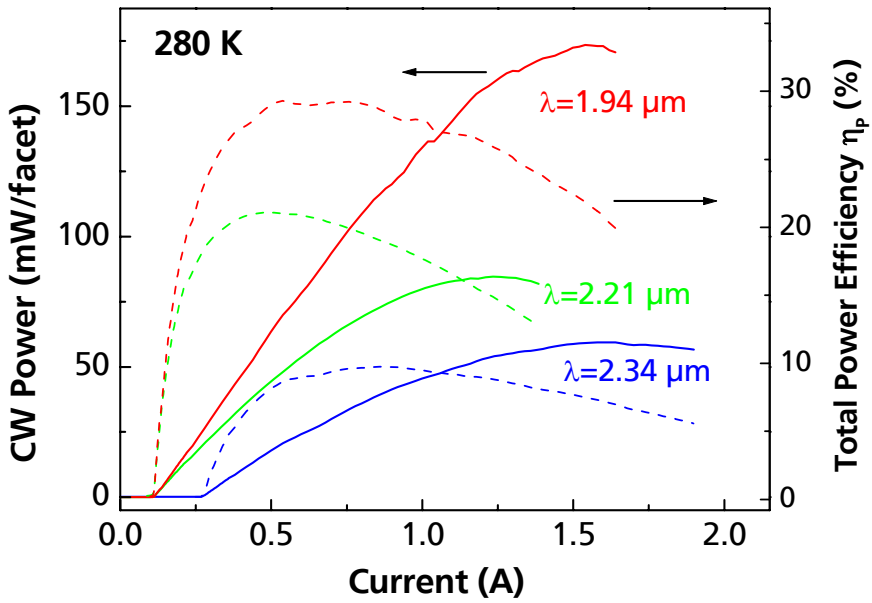


**Fig. 2** Power output (solid lines) and power efficiency vs current (dash lines) characteristics recorded at 280 K heat sink temperature for three lasers emitting at 1.94, 2.21 and 2.34 μm. The 64 μm x 1000 μm ridge waveguide lasers were operated in cw mode.

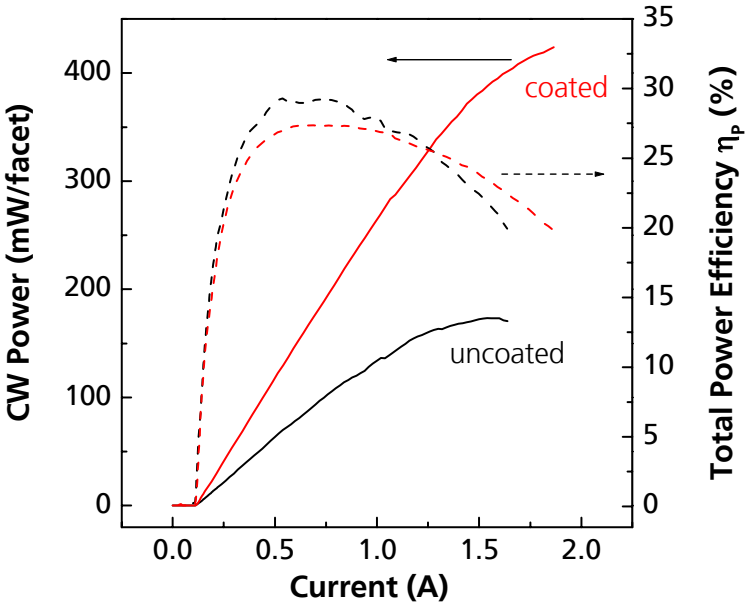


**Fig. 3** 280 K cw power-current (solid lines) and power efficiency-current characteristics (dash lines) of two 64 µm x 1000 µm ridge waveguide lasers with uncoated (black) and HR/AR coated (red) mirror facets. The emission wavelength for both lasers is 1.94 µm.

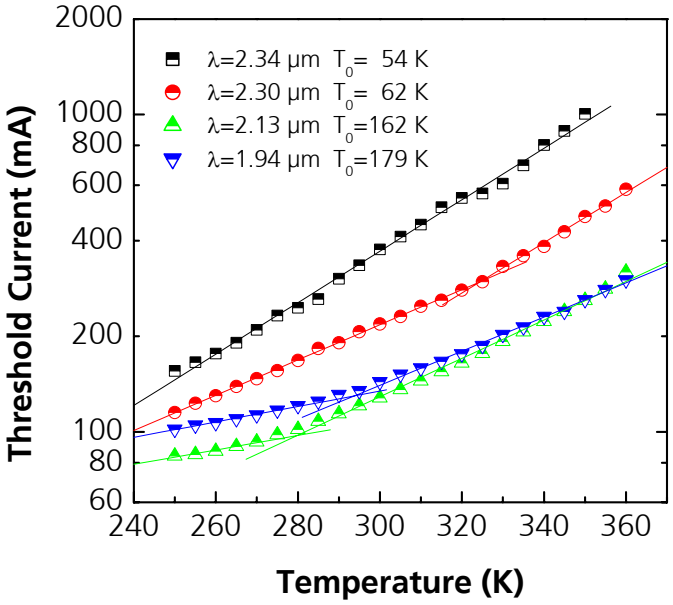


**Fig. 4** Pulsed threshold current vs temperature for four different 64 µm x 1000 µm ridge waveguide lasers emitting between 1.94 and 2.34 µm. The $T_0$ values for the low temperature range are indicated as well.

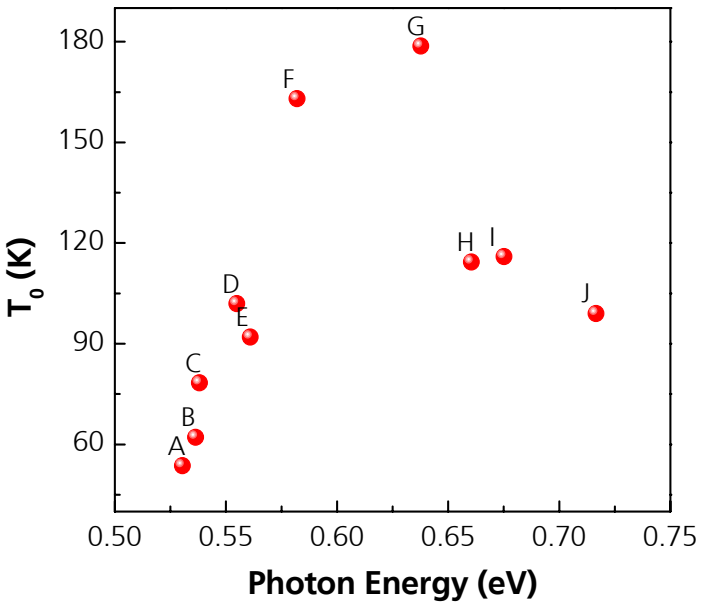


**Fig. 5** Characteristic temperature $T_0$ of the different diode lasers vs emitted photon energy.

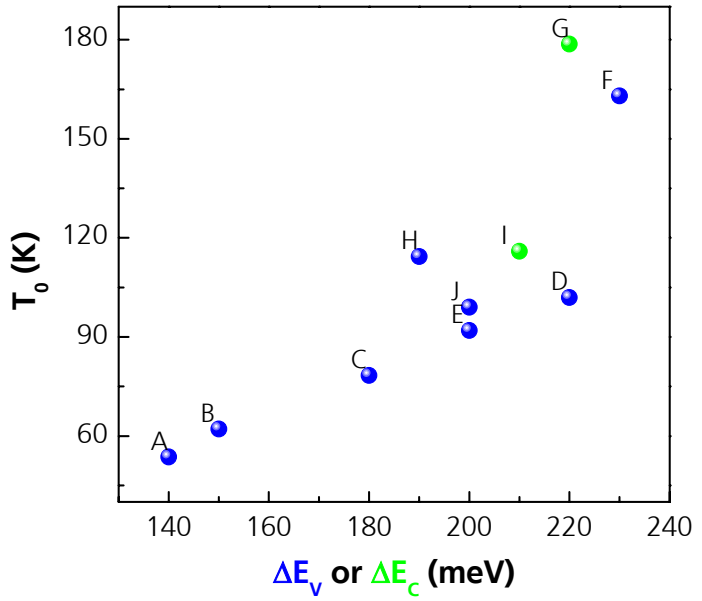


**Fig. 6** Characteristic temperature $T_0$ of the different diode lasers vs the valence band offset $\Delta E_V$ or conduction band offset $\Delta E_C$, whichever is smaller

| Wafer | $\lambda\,(\mu m)$ | $\alpha_i\,(cm^{-1})$ | $\eta_i\,(\%)$ | $J_{th,\infty}\,(A/cm^2)$ |
|---|---|---|---|---|
| J | 1.72 | 19 | 72 | 535 |
| H | 1.87 | 4.2 | 63 | 141 |
| G | 1.94 | 6.1 | 77 | 121 |
| F | 2.13 | 6.1 | 77 | 105 |
| E | 2.21 | 7.7 | 78 | 108 |
| D | 2.23 | 7.6 | 72 | 110 |
| C | 2.30 | 4.1 | 50 | 154 |
| B | 2.31 | 4.6 | 38 | 304 |
| A | 2.34 | 2.7 | 42 | 164 |

**Table I** Internal loss coefficient $\alpha_i$ , internal quantum efficiency $\eta_i$ , as well as threshold current density for infinite cavity length $J_{th,\infty}$ for the various laser diodes with emission wavelengths given in the second column. All the results were obtained for a 64 µm aperture, measured at 280 K.

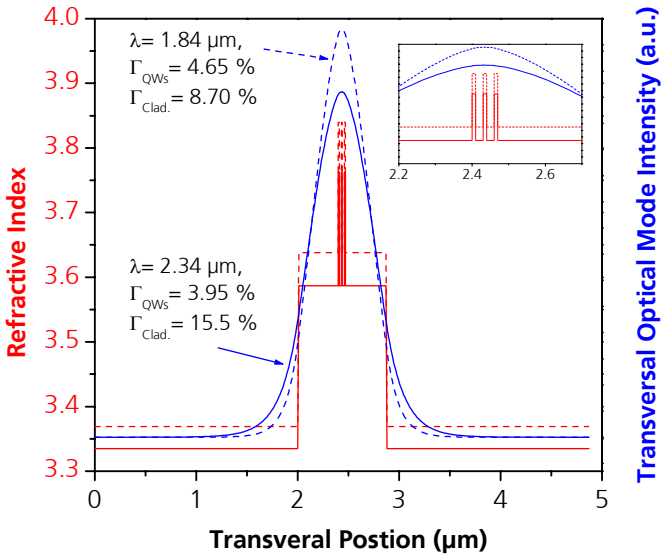


**Fig. 7** Calculated transversal optical mode intensity (right axis) and refractive index (left axis) vs transversal position, corresponding to the growth direction, for two different lasers emitting at 1.84 µm and 2.34 µm. The inset zooms in the QW active region.

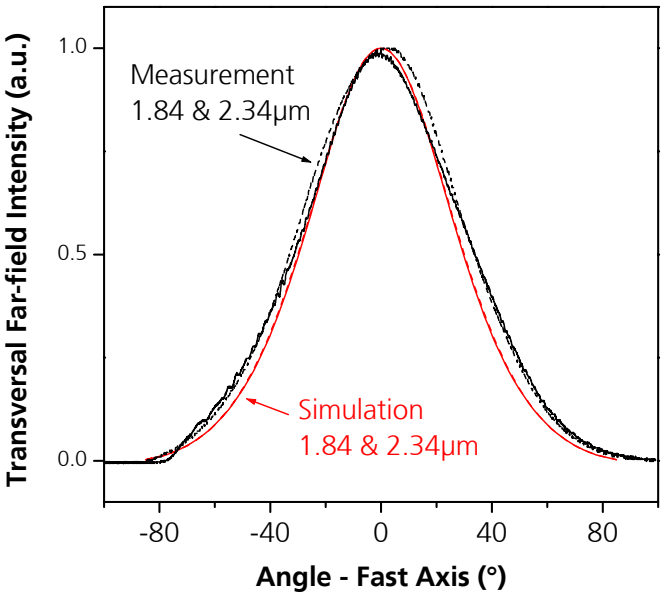


**Fig. 8** Calculated (red) and measured (black) transversal far-field angular distributions for two different lasers emitting at 1.84 µm and 2.34 µm.

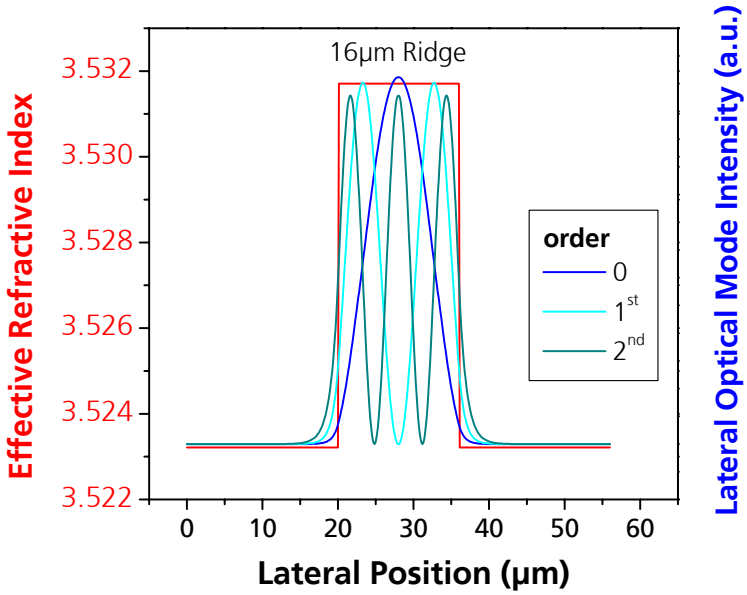


**Fig. 9** Calculated lateral optical mode spatial profiles up to the 2nd order for a 1.94 µm diode laser. The assumed etch depth is ~1.9 µm and the ridge width is 16 µm.

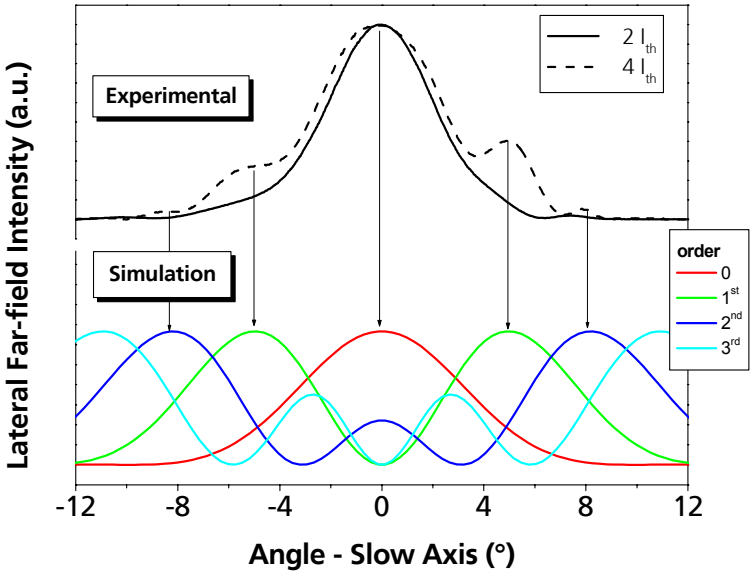


**Fig. 10** Experimental (upper) and calculated (lower) lateral far-field mode profiles of a 16 µm x 1000 µm diode laser with coated mirror facets emitting at 1.94 µm. The experimental data were recorded at room temperature for two different injection currents, $2I_{th}$ and $4I_{th}$, and the calculated angular distribution is up to the 3rd order.

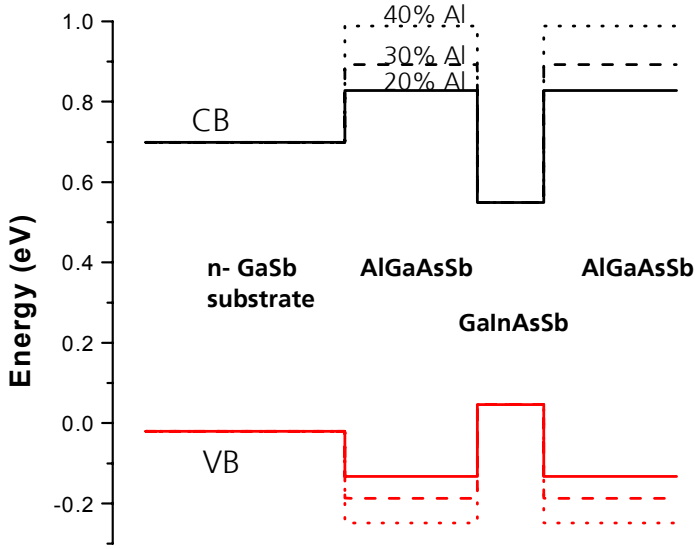


**Fig. 11** Calculated conduction and valence band profile for three different QW laser structures for varying the Al-compositions in the barriers, 20%, 30%, 40%, resulting in different carrier confinement.

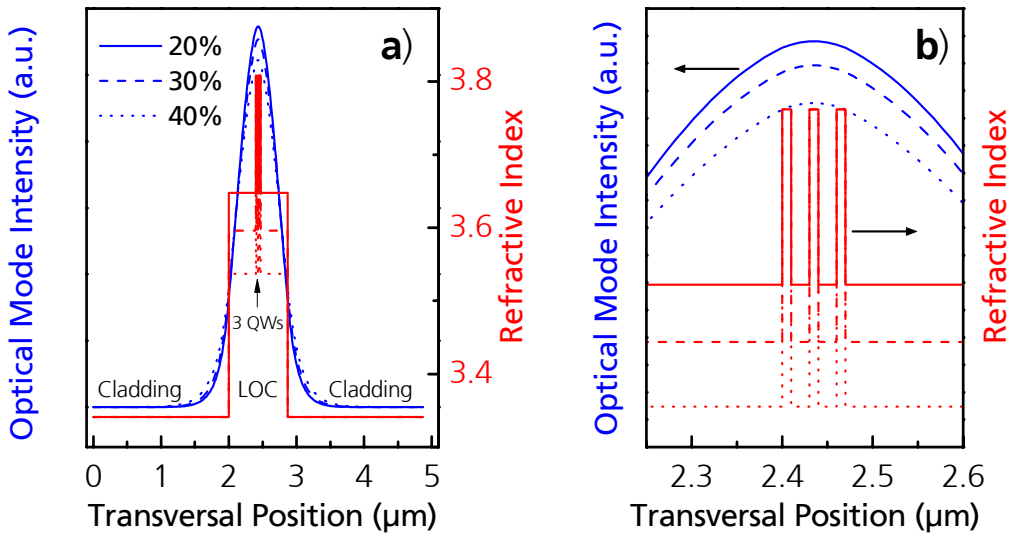


**Fig. 12** a) Calculated transversal optical mode intensity (left axis) and refractive index (right axis) vs transversal position, corresponding to the growth direction, for three lasers with different Al-content, all emitting at 2.23 µm. Plot b) zooms in the QW active region.

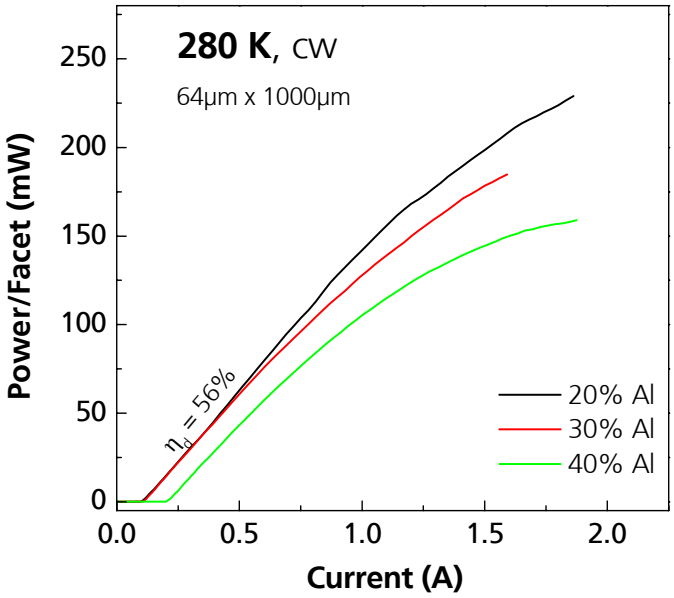


**Fig. 13** CW light output power vs injection current recorded at 280 K for three different lasers with various Al-compositions as indicated, all emitting at 2.23 µm and with 64 µm x 1000 µm geometry.

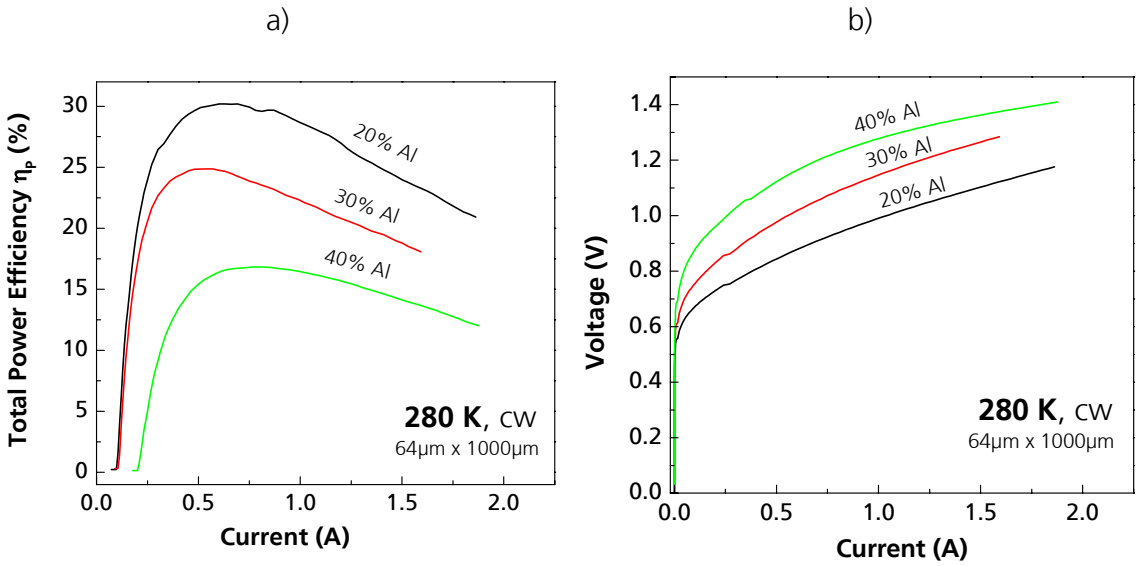


**Fig. 14** Total power efficiency (a) and voltage-current (b) characteristics for three different 2.23 µm lasers with various Al-compositions as indicated. The ridge geometry was 64 µm x 1000 µm and the data was recorded at 280 K.

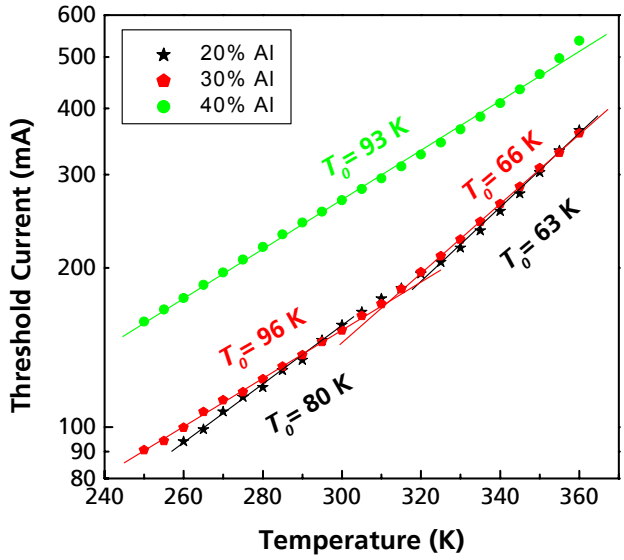


**Fig. 15** Pulsed threshold current vs temperature for three 64 µm x 1000 µm diode lasers with different Al-concentrations, emitting at 2.23 µm. $T_O$ values for the low and high temperature ranges are given.

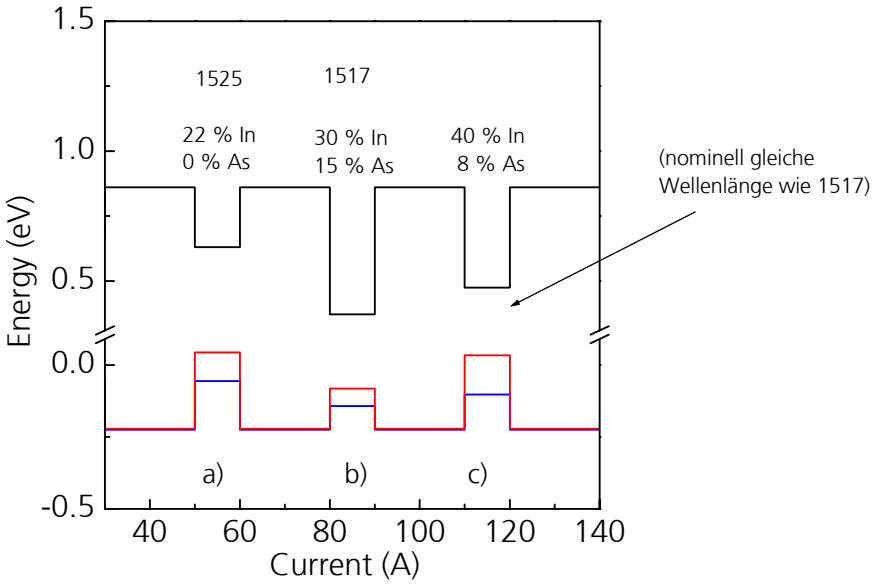


**Fig. 16** Calculated conduction and valence band potential for three different QW lasers. Using the indicated QW composition (b) and (c) emission around 2.4 µm is expected.

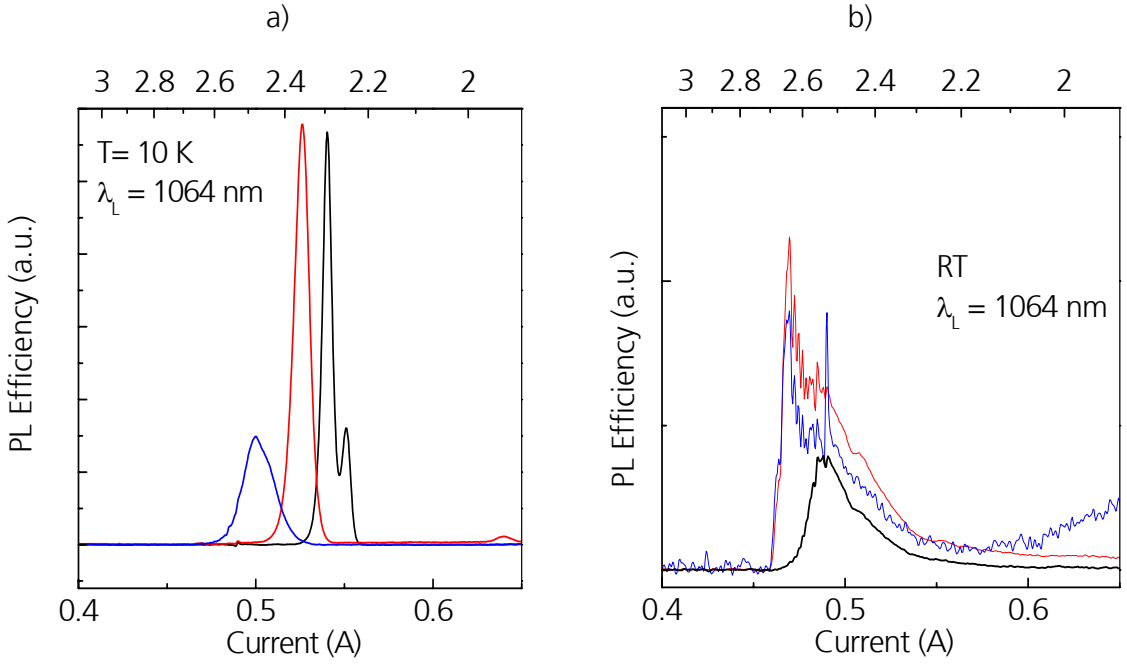


**Fig. 17** 10 K (a) and room temperature (b) photoluminescence spectra of three different laser core test structures with increasing In-content (39, 43, and 48%). The highest In-content structure exhibits strain-relaxation behavior.

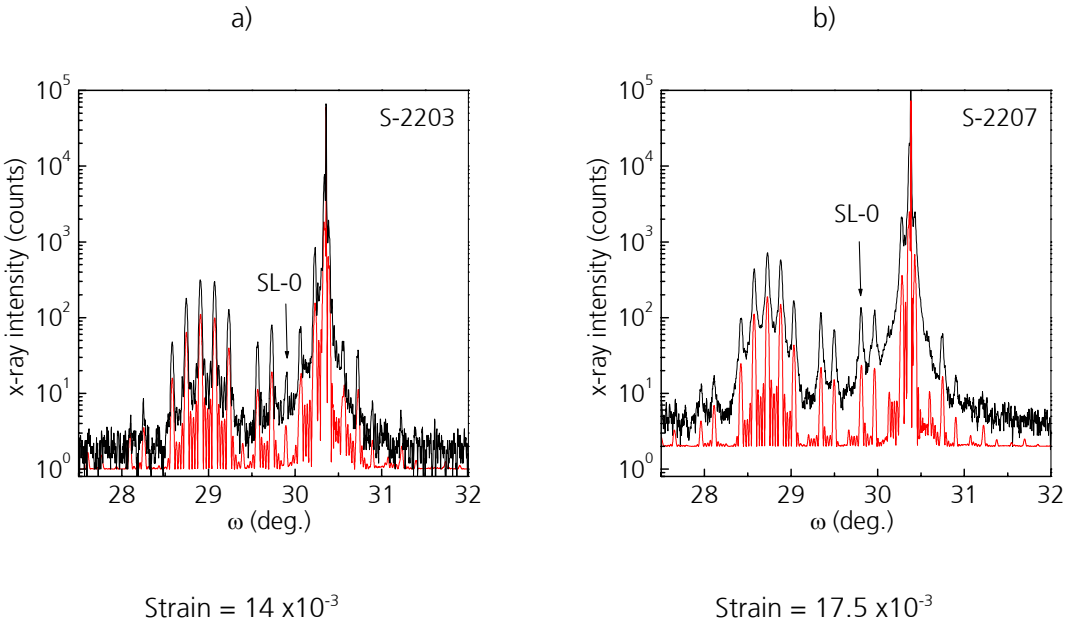


**Fig. 18** Measured and simulated X-ray diffraction profile covering the 004-reflection range of two laser core test structures with different In-content (43 and 48%). The diffractogram b) displays the laser core with 48% In revealing strain-relaxation onset.

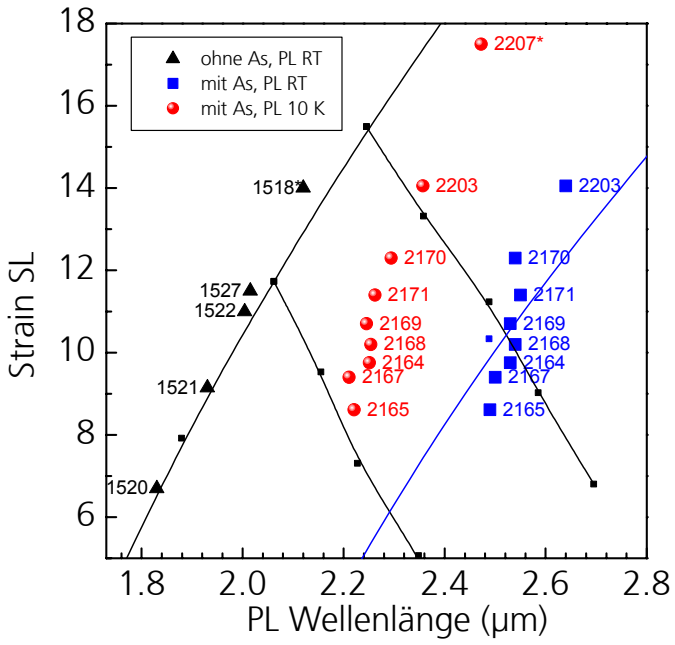


**Fig. 19** Quantum well active region strain vs photoluminescence emission wavelength for various laser core test structures recorded at 10 K as well as at 300 K. The longest PL emission wavelength achieved was 2.64 µm.

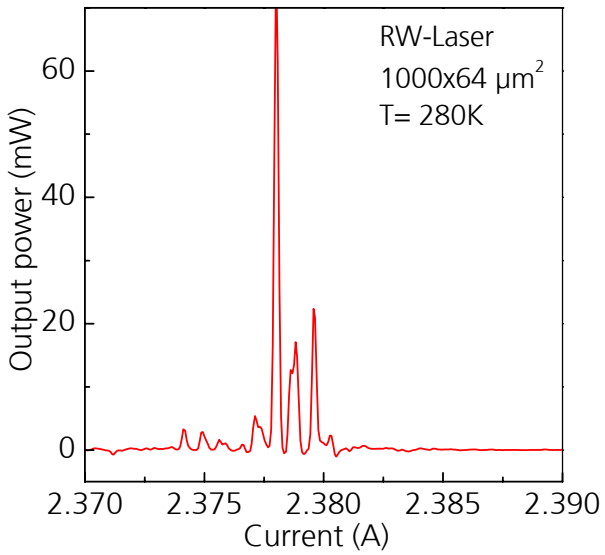


**Fig. 20** 280 K lasing spectrum of a 64 µm x 1000 µm 3 QW diode laser emitting at 2.38 µm.

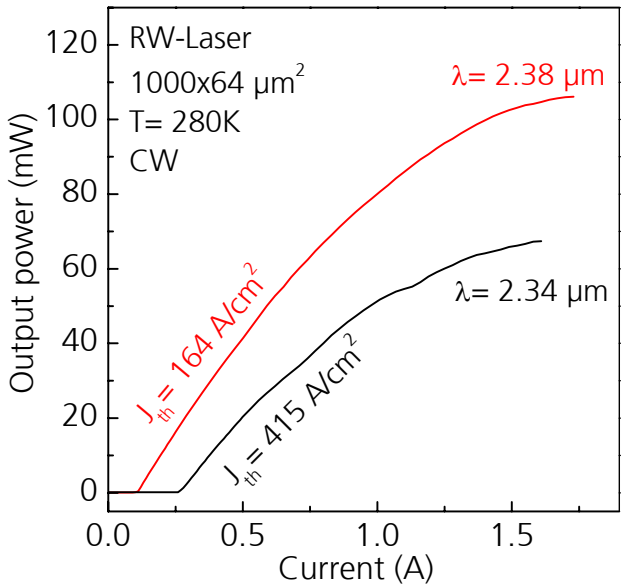


**Fig. 21** Light output characteristic of the present 2.38 µm diode laser, and for comparison the corresponding characteristic of an earlier device emitting at 2.34 µm. Both devices had a 64 µm x 1000 µm geometry and the data was recorded at 280 K.

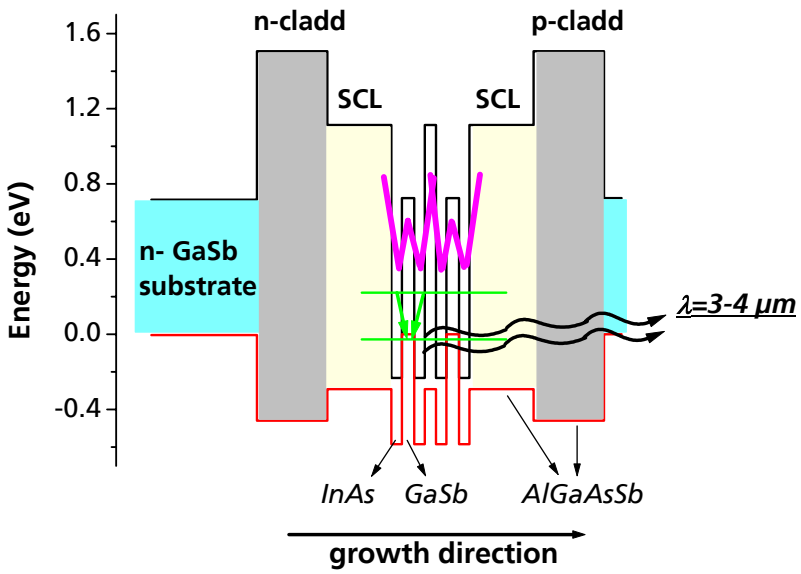


**Fig. 22** Schematic conduction and valence band edge profile of a 5-period InAs/GaSb/InAs/AlGaAsSb type-II W-laser structure.

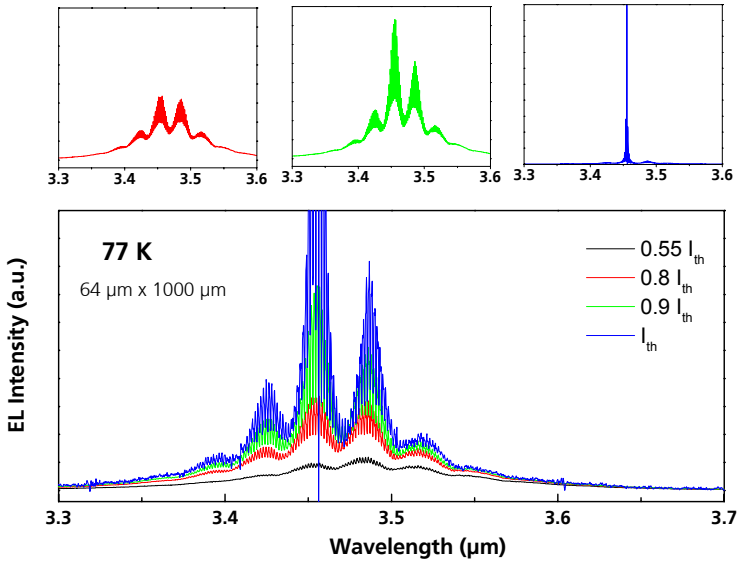


**Fig. 23** 77 K spectral characteristics of a first generation InAs/GaSb/$Al_{0.5}Ga_{0.5}As_ySb_{1-y}$ type-II W-diode laser below and at threshold. The diode laser size was 64 µm x 1000 µm.

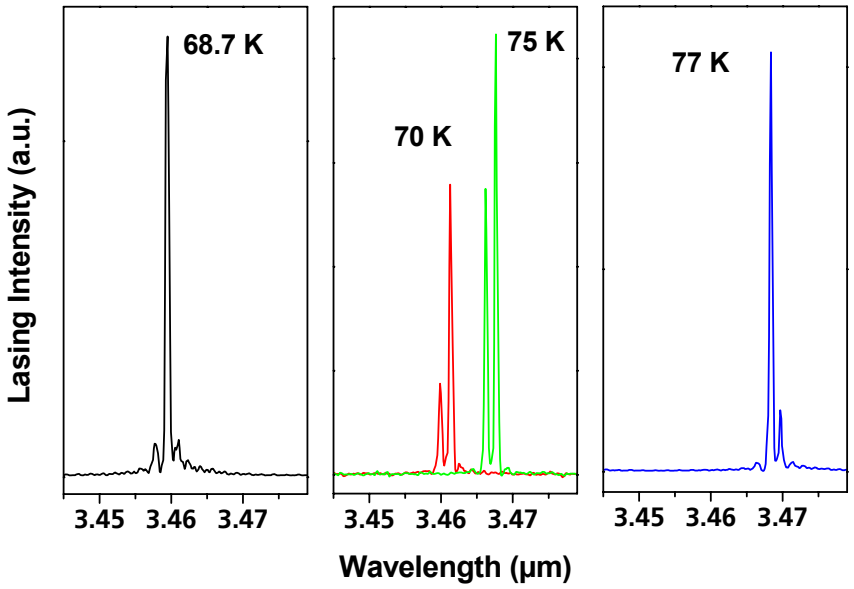


**Fig. 24** Lasing emission spectra of a first generation InAs/GaSb/$Al_{0.5}Ga_{0.5}As_ySb_{1-y}$ type-II W-diode laser, with 64 μm x 1000 μm ridge width and resonator length, respectively recorded at different temperatures.

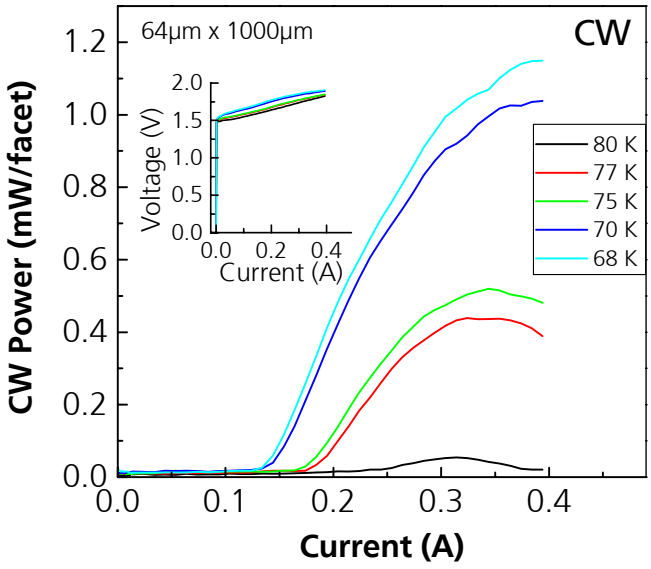


**Fig. 25** CW light output vs injection current at different heat sink temperatures (68 - 80 K), for a first generation W-diode laser with 64 μm x 1000 μm geometry. The inset displays the corresponding voltage-current characteristics.

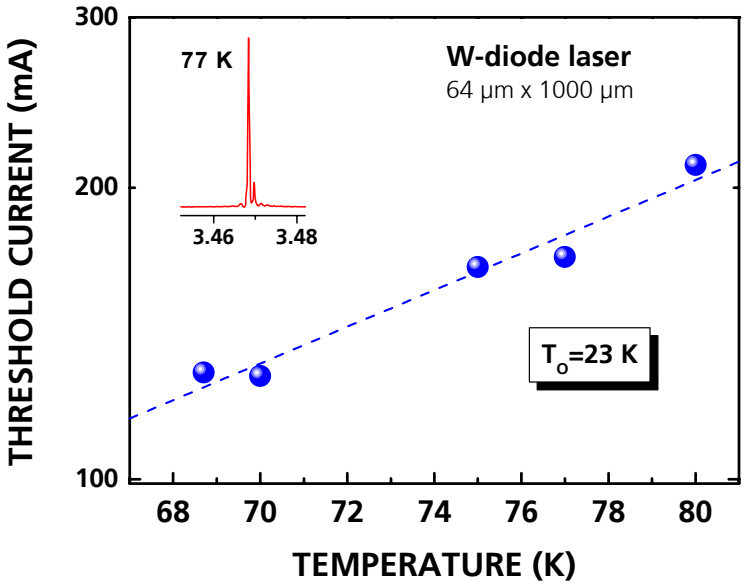


**Fig. 26** Threshold current vs temperature for a first generation W-diode laser emitting at 3.47 µm with a 64 µm x 1000 µm ridge geometry. The characteristic temperature, $T_0$ , amounts to 23 K.

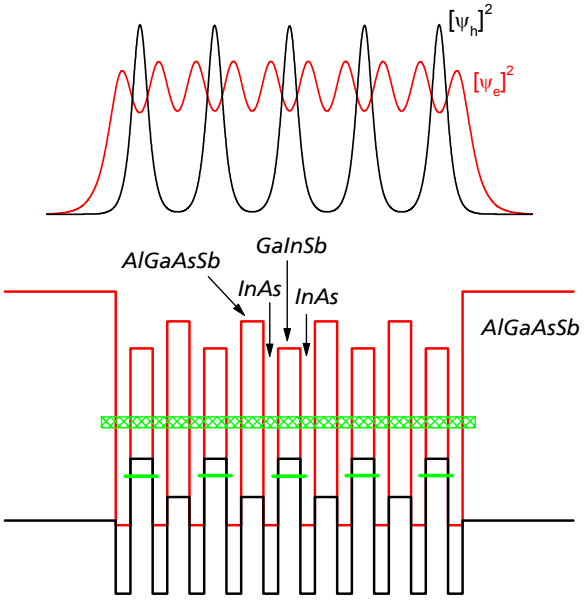


**Fig. 27** Schematic conduction and valence band edge profile of a type-II InAs/GaInSb/ InAs/AlGaAsSb superlattice laser based on bound-to-miniband transition.

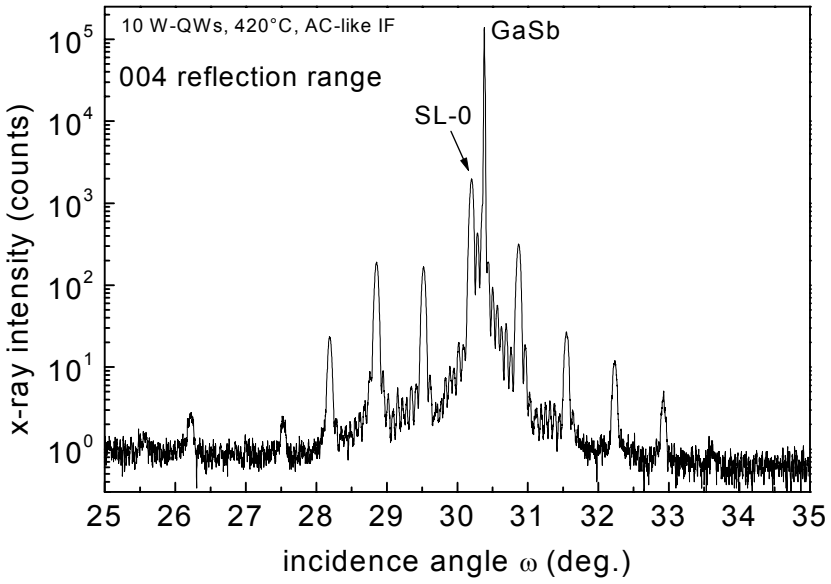


**Fig. 28** Measured X-ray diffraction profile covering the 004-reflection range of GaSb for a 10-period W-laser core layer sequence.

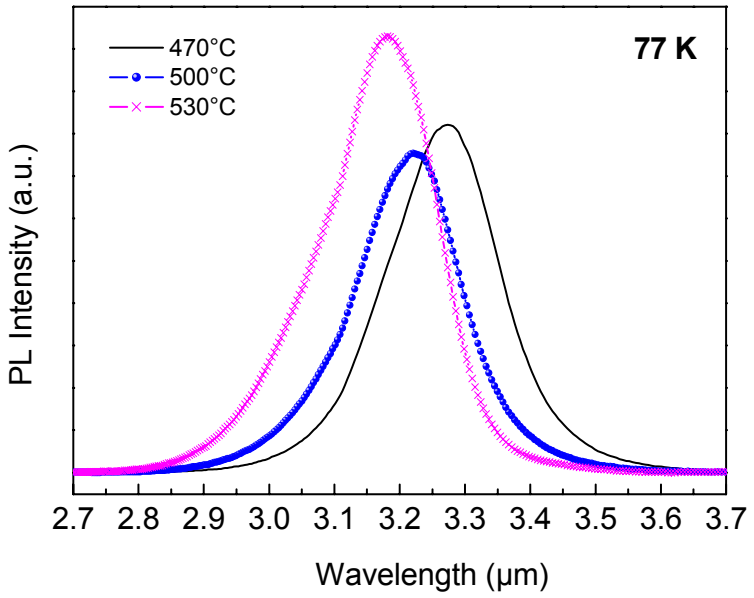


**Fig. 29** 77 K photoluminescence spectra of three different W-laser structures with different upper cladding growth temperature, 530, 500 and 470°C. All three diode lasers consist 5 W-periods and alternating interface sequences.

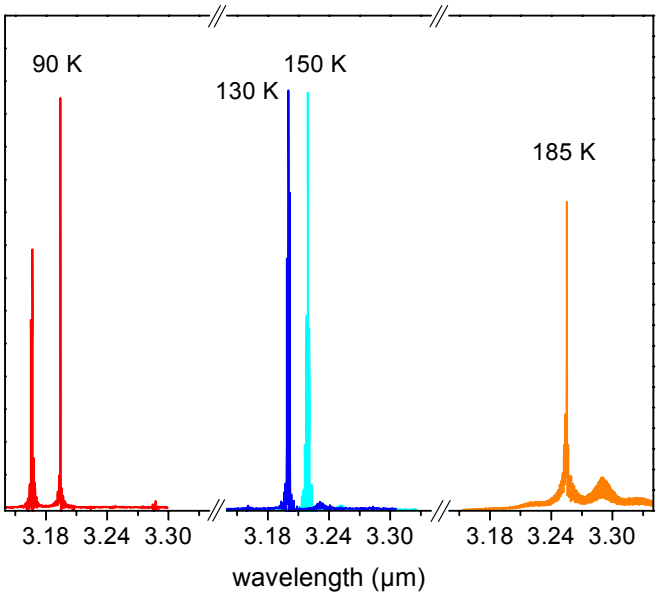


**Fig. 30.** CW lasing emission spectra of an InAs/GaInSb/AlGaAsSb type-II-W diode laser, recorded at different temperatures. A maximum cw operating temperature of 185 K has been achieved. The laser geometry was 64 µm x 1000 µm.

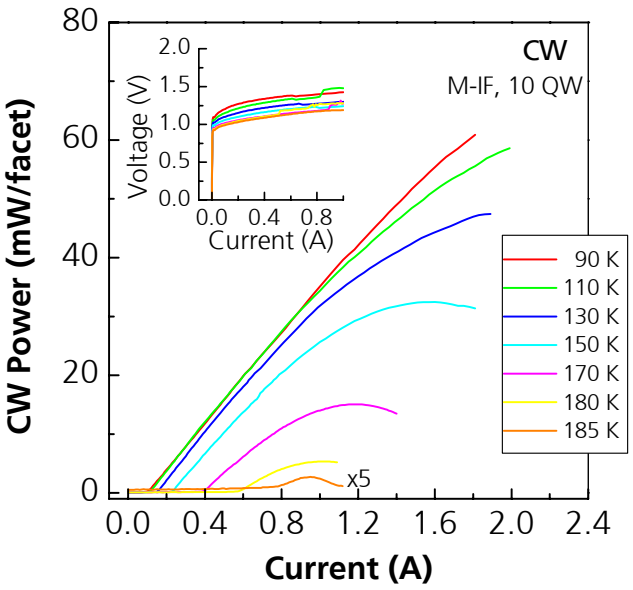


**Fig. 31** CW light output characteristics at heat sink temperatures between 90 and 185 K, of a 10-period W-laser with 64 µm x 1000 µm geometry. The inset displays the corresponding voltage-current characteristics.

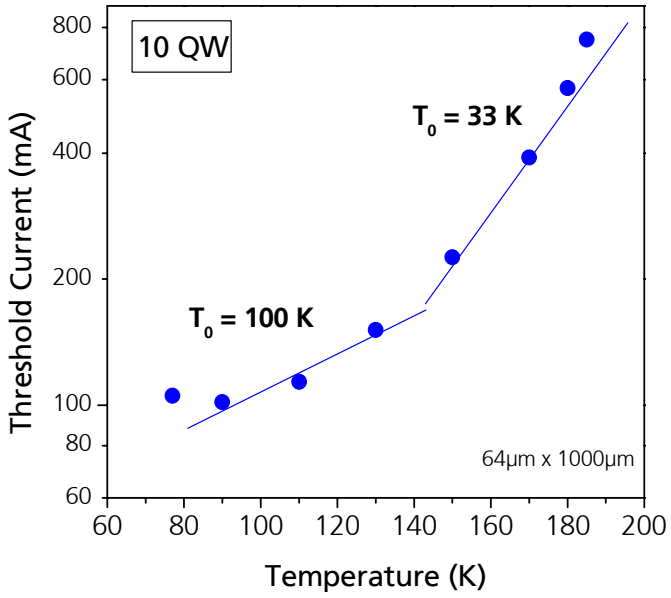


**Fig. 32** Threshold current vs temperature for a 10-period W-diode laser with 64 µm x 1000 µm ridge geometry. The characteristic temperature, $T_0$, amounts to 100 K in the low temperature regime and 33 K in the high temperature range.

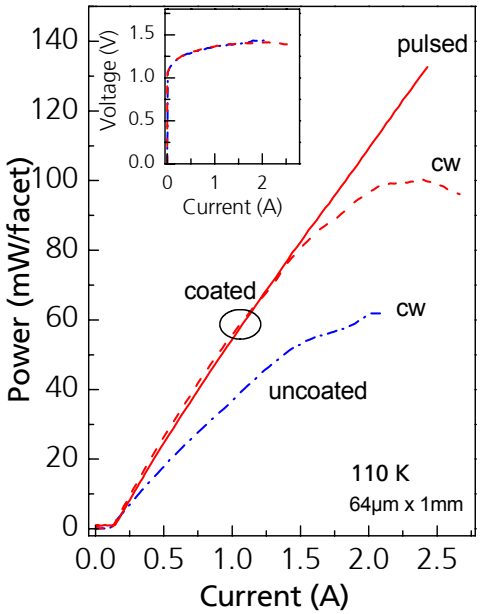


**Fig. 33** Light output characteristics of a 10-period W-diode laser at 110 K with coated mirror facets in cw (dashed curve) and pulsed operation (solid curve), and for comparison without coating in cw mode (dash dotted curve). The laser geometry is 64 µm x 1000 µm.